https://doi.org/10.5194/egusphere-2025-5145
Preprint. Discussion started: 28 October 2025

Assessing Flood-Influenced Sediment Dynamics Using UAV Photogrammetry and Machine Learning: Insights from River Sense, Switzerland.

Nahin Rezwan[1], David Mair[2], Alexander C. Whittaker[1], Fritz Schlunegger[2], Ariel Henrique do Prado[2], Sadia Hossain Setu[3]

[1]Imperial College London, SW7 2AZ, UK; [2]University of Bern, 3012, Switzerland; [3]Centre for Climate Research and Community Empowerment Ltd, IG1 3DB, UK

Correspondence to: Nahin Rezwan (n.rezwan@imperial.ac.uk)

Abstract

Gravel-bed rivers are shaped by complex interactions between hydrological forcing, sediment sorting, and channel morphology, yet fine-scale, spatially continuous observations of these processes remain rare. We combine UAV structure-from-motion photogrammetry with machine-learning grain segmentation to quantify flood-driven sediment redistribution in a minimally disturbed gravel-bed river (Sense River, Switzerland). Two surveys of four gravel bars (2021 and 2024) mapped individual clasts in images at centimetre resolution, allowing spatial and temporal analysis of grain-size patterns. We show clear intra-bar fining from crests to tails and a reach-scale morphology control on sorting: bend-associated bars are moderately to well sorted, while straight reaches are more poorly sorted. Grain-size distributions converge to self-similar forms across all bars, with analysis of ca. 1.86 million grains providing unprecedented empirical validation of scale-invariant sorting, an improvement by orders of magnitude over conventional pebble counts. To understand the detailed hydraulic controls during the moderately large flood captured between surveys (ca. 180 m³/s; ca. 2-10 years recurrence), we performed detailed hydraulic modelling for one bar, estimating spatial fields of shear stress, Shields parameter, and stability conditions during the flood. We also differentiated the topography between the two surveys to map the relative elevation change. The crest and margin armour remained largely stable, whereas the tail part was extensively reworked. A hydraulically driven mobilisation model reproduced observed mobility with ca. 65% overall accuracy (up to 82% in tails) but under-predicted movement on crests. We also show that where floods were large enough to mobilise the grains, coarse patches were rapidly buried or completely replaced, demonstrating that local hydraulic geometry can override patch stability. Overall, bar adjustment was deposition-dominated for that bar, consistent with the waning stage of the flood, during which reduced shear stresses promoted net deposition. Our data indicates that flows <200 m³/s can remobilise large bar areas, and analysis of gauging data for the Sense River since 1928 shows that such events are becoming more frequent. Our results highlight the important geomorphic role of moderate to moderately large floods in such

https://doi.org/10.5194/egusphere-2025-5145
Preprint. Discussion started: 28 October 2025

rivers and demonstrate high-resolution, hydraulically informed grain mapping as a robust tool for predicting gravel-bed river response under changing flood regimes.

1 Introduction

Gravel-bed rivers are among the most dynamic components of fluvial landscapes, continuously adjusting their morphology in response to fluctuations in hydrological regime and sediment supply (Buffington & Montgomery, 2013; Church, 2002, 2006; Parker, 1990). These river systems self-organise through dynamic interactions among flow competence, sediment supply, bed material texture, and channel geometry (Ashmore & Rennie, 2013; Church, 2002, 2006). These processes establish a metastable equilibrium that can be frequently interrupted by external forces such as floods or changes in sediment supply (Ashmore & Rennie, 2013; Buffington & Montgomery, 2013). Understanding the behaviour of these rivers is important for constraining sediment dynamics (Montgomery & Buffington, 1997; Parker, 1990), sustaining riverine ecosystems (Chessman et al., 2006; Gurnell et al., 2012, 2016; Steiger et al., 2005), river management and restoration (Brierley et al., 2006; Chessman et al., 2006; do Prado et al., 2024; Newson & Large, 2006), and mitigating flood hazards (Lane et al., 2007; Surian et al., 2016). Gravel-bed rivers, in particular, function as connectors between zones of erosion and deposition, regulating sediment flux through remobilisation cycles and sediment preservation (Dingle et al., 2020). Effective management must recognise their inherent dynamism and process-driven nature, rather than treat them as static engineering problems (Beechie et al., 2010).

Floods can drive major geomorphic transformation in fluvial systems, acting as principal agents that reconfigure channels, redistribute sediments, and reshape ecosystems (Gurnell et al., 2012; Lane et al., 2007; Phillips & Jerolmack, 2016; Surian et al., 2016). Moderate-sized floods, such as those recurring over interannual to decadal timescales, are argued to be particularly effective in constructing, modifying, and remobilising gravel bars, facilitating both surface and subsurface sediment exchanges (Ashworth et al., 1992; Habersack et al., 2001; Madej, 1999; Surian et al., 2016). Classic sediment transport models often rely on threshold-based approaches, such as the Shields criterion, to predict grain entrainment and transport capacity (Wilcock & Crowe, 2003). However, actual sediment dynamics at the bar scale remain highly variable, driven by complex interactions between flow hydraulics, grain-size distribution, bar morphology, and sediment availability (Bertoldi et al., 2010; Rice & Church, 2010; Schlunegger et al., 2020). Importantly, gravel-bed riverbeds are rarely homogeneous; rather, they are composed of discrete grain-size patches whose stability and response to hydraulic forcing vary substantially at bar and sub-bar scales. Capturing the formation, persistence, and

https://doi.org/10.5194/egusphere-2025-5145
Preprint. Discussion started: 28 October 2025

remobilisation of these patches is essential for understanding the selective transport of sediment and the spatial complexity of channel morphodynamics (Paola & Seal, 1995; Vericat et al., 2017).

Historically, our understanding of sediment dynamics and gravel bar reworking in these systems has depended heavily on field sampling and conventional imagery techniques (Ashworth et al., 2000; Church & Hassan, 1992; Warburton & Davies, 1994). While these traditional approaches have been important for establishing key principles in river research, their limited spatial coverage and temporal resolution, as well as potential operator bias, present challenges for capturing the full complexity of fine-scale sedimentary dynamics (Carbonneau et al., 2004; Rice & Church, 2010). The advent of unmanned aerial vehicle (UAV)-based photogrammetry has significantly advanced river morphodynamics research, providing spatially extensive, high-resolution datasets of river topography and sediment characteristics (James & Robson, 2012; Patel et al., 2025; Woodget & Austrums, 2017). Complementing UAV photogrammetry, recent developments in machine learning enable automated and objective segmentation and measurement of sediment grain sizes, significantly enhancing analytical accuracy and reproducibility (Buscombe, 2013; Garefalakis et al., 2023; Mair et al., 2022, 2024; Vázquez-Tarrío et al., 2017; Woodget et al., 2015).

These technological advancements present opportunities to address notable gaps in river science, such as the detailed assessment of flood impacts on sediment redistribution, accurate reconstruction of paleohydraulic conditions, and improved understanding of sediment dynamics in space and time (Javernick et al., 2014; Mair et al., 2024; Wheaton et al., 2010). Nevertheless, to date many existing studies have primarily focused on technical and logistical aspects of data acquisition and processing rather than explicitly addressing sedimentary processes and geomorphic implications (Javernick et al., 2014; Woodget & Austrums, 2017). Consequently, considerable potential remains to utilise these technologies for fundamental fluvial research into sediment redistribution, grain-size variability, and sediment stability thresholds during hydrological events. A major unresolved issue involves the spatial integration of grain-size distributions and topographic changes resulting from known flood events. While studies tend to focus exclusively on grain-size variation (e.g., textural patches or armouring effects) or on topographic changes (erosion-deposition patterns), few simultaneously capture both aspects at comparable resolution. Bridging this gap requires datasets that integrate high-resolution topography and grain-size distributions, thereby enabling detailed analyses of how hydraulic conditions override or interact with sedimentological controls.

https://doi.org/10.5194/egusphere-2025-5145
Preprint. Discussion started: 28 October 2025

This study directly addresses this research need by evaluating spatial and temporal sedimentary responses in an unmodified gravel-bed river, the Sense River, Switzerland, including a well-documented post-flood event (approximately a 2-10-year return period) on November 14, 2023 (FOEN, 2024). We apply UAV-based photogrammetry combined with automated machine learning techniques to map sediment grain sizes and topographic changes at sub-centimetre resolutions. We characterise the hydraulic conditions resulting in the sediment mobilisation and deposition across gravel bars in the studied system and how these are conditioned by sediment grain-size distributions. Such information enables us to quantify how sediment patches of differing texture and morphology respond to hydraulic forcing, and we explore how these dynamics might evolve due to ongoing climate change in the region. By addressing these points, our study aims to improve predictions of sediment dynamics, inform river management strategies, and advance the broader understanding of geomorphic processes in gravel-bed river systems.

2 Study area: Sense River, Switzerland

The Sense River is located in western Switzerland and is one of the few rivers in the country that has remained largely pristine, maintaining a dynamically active gravel-bed morphology (Tonolla et al., 2021) (Fig. 1a, b, c, d, e). Flowing approximately 35 km from its headwaters in the Alpine foothills near Zollhaus (i.e., the confluence of its major feeders, the Kalte and Warme Sense), it joins the River Saane near Laupen (Tonolla et al., 2021). The Sense catchment, covering approximately 435 km² and characterised by steep slopes, forested valleys, and agricultural landscapes, receives an average annual rainfall of 1345 mm, with the maximum monthly precipitation typically occurring in August and the minimum in February (Tonolla et al., 2021). Unlike most Swiss rivers, which have been heavily channelised or engineered for flood protection, water supply, and hydroelectric power generation, the River Sense retains much of its original planform, including actively migrating channels and gravel bars (Arnaud et al., 2015, 2019; do Prado et al., 2024; Hohensinner et al., 2021; Tonolla et al., 2021). This geomorphic authenticity makes it an excellent natural laboratory for studying river dynamics, sediment transport, and flood impacts on gravel-bar morphology and grain-size distributions. Gravel bars in the river display diverse morphologies and sorting characteristics (do Prado et al., 2025a, b), reflecting active sediment supply (approximately 7,500 m³/yr from the Kalte and Warme Sense; GEKOBE, 2014).

https://doi.org/10.5194/egusphere-2025-5145
Preprint. Discussion started: 28 October 2025

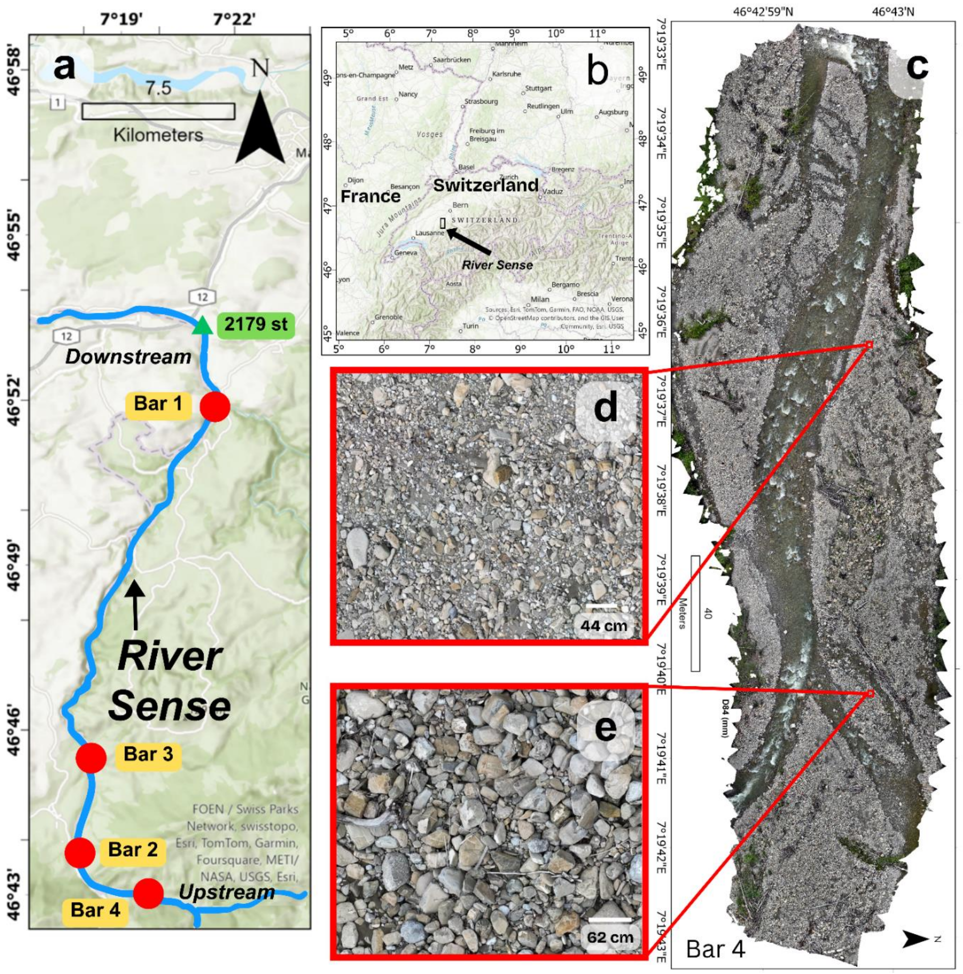

Figure 1: (a) The study area map illustrates the Sense River catchment in western Switzerland, highlighting the four surveyed gravel bars (Bar 1, Bar 2, Bar 3, and Bar 4) in red circles along the channel and the Thörishaus, Sensematt 2179 hydrographic station in a green triangle. Panel (b) shows the location of the Sense in western Switzerland. Panel (c) presents an overview of a typical gravel bar, while panels (d) and (e) display representative images of bar surface sediment textures.

The hydrological regime of the River Sense is typically dominated by seasonal snowmelt in late spring and early summer and rainfall-driven flood events, resulting in marked fluctuations in discharge throughout the year (Viviroli & Weingartner, 2004; Weingartner & Aschwanden, 1994). Hourly discharge and water-level data, continuously recorded by the Swiss Federal Office for the Environment (FOEN) from 1928 to 2025, provide an exceptional basis for

https://doi.org/10.5194/egusphere-2025-5145
Preprint. Discussion started: 28 October 2025

analysing flood frequency, magnitude, duration, and seasonality, and for comparing contemporary events with the historical flood record (Fig. 2a).

Moderate- to high-magnitude floods have been regularly recorded in the Sense River over the past century, reshaping channel patterns, mobilising gravel bars, and impacting surrounding infrastructure and communities. One such event occurred on 14 November 2023, with a peak discharge of approximately 180 m³/s (Fig. 2b). We use the term “moderately large” to define the discharge level in this work, as according to the Federal Office for the Environment (FOEN, 2025), this flood corresponds to a return period between 2 and 10 years, classifying it as a moderate but significant event, well above annual peaks but below rare catastrophic floods. Despite its moderate magnitude, this flood event provided a unique opportunity to directly observe and quantify sediment transport processes and geomorphic changes under natural conditions. This is because floods of this return period class are often considered bankfull events, typically capable of mobilising a wide range of grain sizes (Church, 2006; M. Wolman & Leopold, 1957).

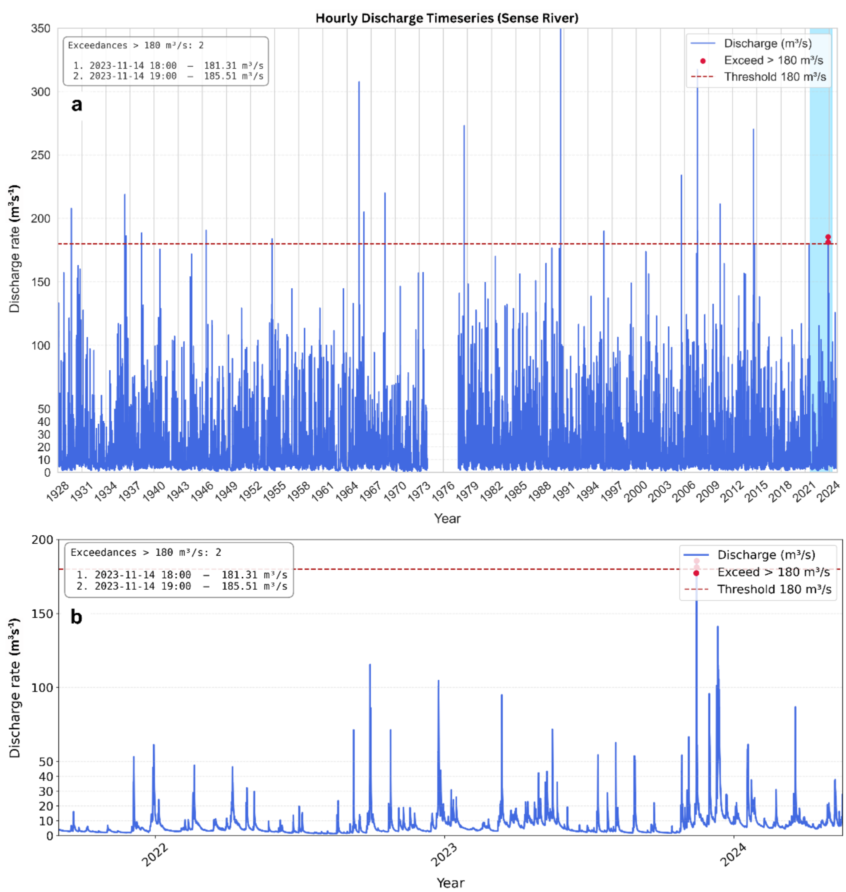

https://doi.org/10.5194/egusphere-2025-5145
Preprint. Discussion started: 28 October 2025

Figure 2: (a) Continuous hourly discharge time series from 1928-2025, with shaded bands marking the periods of UAV field surveys. We highlight major flood events exceeding the key discharge threshold of 180 m^3/s (red dashed line) discussed here, including the November 14, 2023 flood analysed in this study. (b) Hydrograph between the two surveys from September 30, 2021, to May 17, 2024, including the November 2023 flood. This time portion corresponds to the light blue shading in (a).

3 Methods

We selected four distinct gravel bars (Fig. 1a, c, d, e) along the Sense River as representative field sites based on their accessibility and geographic location. Our dataset consists of two UAV-based field campaigns conducted on four distinct gravel bars of the River Sense (Fig. 1a, c-e). The first survey was carried out on September 30, 2021 (c.f. do Prado et al. 2025a, b), and we conducted the second survey on May 17, 2024. This captured the post-flood conditions following a major event on 14 November 2023, with a peak discharge of ca. 180 m^3/s (Fig. 2b). This flooding event was ca. 50% larger in peak discharge than any other floods recorded during the interval between the two field campaigns. We combined hydrological analysis, high-resolution topographic surveying, 3D surface reconstruction, automated grain-size measurement, and hydraulic modelling to quantify both spatial and temporal dynamics of the bars and to characterise and quantify flood-induced changes in bar morphology and sedimentology, as we explain further below.

Although we mapped grain size and surface changes across all four bars, our detailed temporal analysis focused on the part of Bar 3, which offered the greatest spatial and temporal overlap between surveys and is situated 16 km upstream from the hydrographic station (Sense-Thörishaus, Sensematt 2179) (Fig. 1a). Bar 1, despite its proximity to the gauge, was excluded from temporal analysis due to its near-complete removal during the 2023 flood. Each of these core methods is described in detail in the subsequent sections: UAV-based photogrammetry, machine learning-based grain size segmentation and measurement, hydraulic parameter estimation, hydrological and climate trend analysis, zone-wise normalisation, and comparative metrics analysis.

https://doi.org/10.5194/egusphere-2025-5145
Preprint. Discussion started: 28 October 2025

3.1 UAV-based photogrammetry

3.1.1 Field survey

We carried out high-resolution aerial surveys of the gravel bars using a UAV (DJI Mavic 3 Pro enterprise edition) equipped with a 20-megapixel RGB camera and a GNSS module with real-time kinematic (RTK) positioning (Fig. 3a). We selected our survey windows to ensure consistent weather conditions to minimise image artefacts and avoid biases due to shadow or glare. Our survey design maximised spatial coverage and resolution, ensuring that each flight achieved at least 70% image overlap, an important requirement for Structure-from-Motion (SfM) photogrammetry (Westoby et al., 2012) at a fixed altitude of 10 m above ground level. Each field campaign yielded approximately 2,000 images per survey, producing imagery with a ground resolution of 5 mm per pixel. For RTK positioning, we used the online Swipos-GIS/GEO signal that has a horizontal precision of 2 cm and a vertical precision of 4 cm (for 2σ) (Swisstopo, 2025).

3.1.2 Photogrammetric processing

We processed the UAV imagery using the Agisoft Metashape Professional (v1.6) software licensed to the University of Bern, following the standard workflow to ensure reproducibility and model accuracy (Eltner et al., 2016; Fonstad et al., 2013; James et al., 2020). First, we imported and quality-checked all images, discarding those below a sharpness threshold of 0.5 (Fig. 3b). We then performed high-accuracy camera alignment, typically generating between 4,000 and 6,000 tie points and 40,000-60,000 key points per image (Fig. 3b). We further refined the alignment by removing misaligned or low-quality images and optimised camera parameters. We reviewed tie point covariance and excluded any images or points exhibiting excessive covariance to further reduce spatial error.

We improved the photogrammetric models by removing problematic images manually and filtering tie points with high covariance, followed by optimising the point cloud to ensure robust reconstructions. From these point clouds, we created digital surface models (DSMs) at 1 cm per pixel resolution, using interpolation to fill small data gaps (Fig. 3c). Finally, we produced high-resolution orthomosaics from the DSM surfaces (Fig. 3c, d), enabling hole-filling to ensure complete surface coverage and achieving a final orthophoto resolution of 5 mm per pixel.

https://doi.org/10.5194/egusphere-2025-5145
Preprint. Discussion started: 28 October 2025

3.2 Grain segmentation and size measurement

We subdivided each orthoimage into 5 m² image tiles to maximise computational efficiency and enable high-resolution spatial analysis across all surveyed bars (Fig. 3e). Using the ImageGrains tool (Mair et al., 2024), we applied a machine learning-based (ML) approach to segment and measure individual grains from the orthophotos and to determine grain size distributions across all surveyed gravel bars (Fig. 3f). ImageGrains relies on a convolutional neural network (Stringer et al., 2021), trained on diverse gravel-bed imagery, to accurately delineate grain masks and reduce segmentation error (Mair et al., 2022, 2024). For every analysis tile (5 m × 5 m), we applied an area-by-number grain-size measurement method by segmenting and measuring all visible grains (Bunte & Abt, 2001; Butler et al., 2001), recording the lengths of their principal axes (a and b) in millimetres. To ensure consistency and reliability, we only considered grains larger than six pixels (≈30 mm), a threshold aligned with the model and the image resolution.

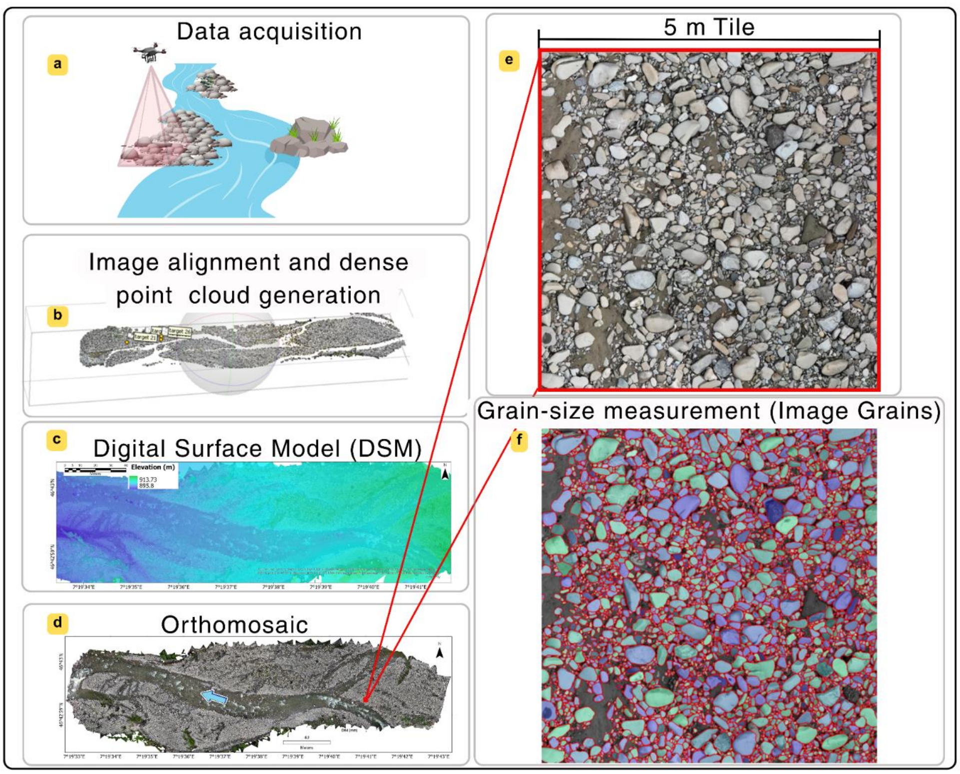

Figure 3: Multi-stage workflow and grain-size analysis: (a) UAV-based image data acquisition; (b) image alignment and dense point cloud generation; (c) digital surface model (DSM) generation from the point cloud; (d) orthomosaic

https://doi.org/10.5194/egusphere-2025-5145
Preprint. Discussion started: 28 October 2025

generation; here the blue arrow shows the flow direction. Panels (e-f) show a 5 m orthophoto tile of a gravel bar surface and corresponding automated segmentation using ImageGrains, where detected grain masks and measured clasts are highlighted.

From these segmented grains, we extracted key statistical descriptors of the grain-size distribution, including the 16th (D16), 50th (D50), 84th (D84), and 96th (D96) percentiles for each tile (GRANT et al., 1990; MacKenzie et al., 2018; Schlunegger et al., 2020). To quantify uncertainty, we applied a bootstrapping approach, resampling measured grains within each tile to generate 95% confidence intervals for grain size estimates in each percentile (Efron & Tibshirani, 1986; Mair et al., 2022). The distribution of grain sizes for each bar is presented as a cumulative distribution function (CDF), facilitating a comparison of fining or coarsening patterns between bars. Additionally, we represented the grain size distributions in terms of the self-similar variable, $\xi = (Dx - D_{mean})/D_{mean}$, following the framework of Fedele & Paola (2007), which computes individual grain size measurements D_x relative to the characteristic sample mean D_{mean}, enabling comparison across diverse sediment populations and highlighting universal patterns in grain sorting irrespective of absolute size. To assess the influence of bar morphology and flood impact, we evaluated temporal variations in absolute grain size and evaluated the sensitivity of both the median and coarser fractions to distinct morphological zones, namely, crest, middle, and tail, across the bar. We assigned each measurement tile to one of these three zones based on its spatial position within the bar, enabling a structured comparison of sediment response in different geomorphic settings.

3.3 Hydraulic parameter estimation

To quantify the hydrodynamic controls on sediment mobility, we focused on Bar 3, and we estimated hydraulic parameters at the tile scale (e.g., every 5 m), using the reconstructed DSMs, field observations, and hydrological records. We calculated the relative elevation change, which we determined by differencing the DSMs derived from the UAV surveys. To account for potential vertical datum offsets or systematic elevation errors between the surveys, we normalised each DSM by subtracting the 75th percentile elevation value (computed across all tiles) of that dataset, a relative alignment that emphasises spatial patterns of elevation change while minimising biases in absolute elevation (Minár et al., 2024; Schwanghart & Scherler, 2017). The resulting map of relative elevation change provides the spatial distribution of bar-scale geomorphic dynamics attributable to the flood event.

Next, we extracted local bed slopes for each tile to characterise the hydraulic gradients. For every measurement tile, we calculated the bed slope as the difference in normalised elevation

https://doi.org/10.5194/egusphere-2025-5145
Preprint. Discussion started: 28 October 2025

between adjacent downstream tiles, divided by the horizontal spacing. This method captures the spatial variability of the bar topography and flow direction, enabling tilewise assignment of slope values. Here, we assume that the steepest downslope direction of each tile aligns with the dominant flow direction during the flood.

Water depth was determined using two sources of information: direct field observations of maximum bankfull stage (e.g., 2 m) on November 14, 2023, identified from flood debris lines and wrack deposits, and hourly water level data from the Federal Office of Environment (FOEN) hydrograph at the Sense 2179 station. We interpolated the peak floodwater surface across the study area using these records and subtracted the DSM elevations for each tile to yield local water depth at the time of the peak flow, making the simplifying assumption that the floodwater surface had negligible topography. With local bed slope and water depth in hand, we estimated the spatial distribution of bed shear stress (τ) during the peak flood for each tile using the standard depth-slope product.

$$\tau = \rho g h S \qquad (1)$$

where ρ is the density of water (1000 kg/m³), g is gravitational acceleration (9.81 m/s²), h is the tilewise water depth (m), and S is the bed slope. This formulation quantifies the hydraulic force available to mobilise sediment at each tile during the flood.

To evaluate the mobility of the sediment, we calculated the Shields parameter (τ*) as:

$$\tau \quad = \frac{\tau}{(\rho_s - \rho) \times g \times D_{50}} \qquad (2)$$

where $\rho_s$is the sediment density (assumed 2650 kg/m^3), and D_{50} is the median grain size for each tile during the first survey. The Shields parameter represents the non-dimensional shear stress and is widely used to calculate the transport of sediment in fluvial environments (Buffington & Montgomery, 1997). Finally, we assessed sediment mobilisation by comparing the calculated Shields parameter at each tile to a theoretical critical value for incipient motion of gravel ($\tau_{cr} = 0.06$) (e.g. Buffington & Montgomery, 1997; Shields, 1936). We further estimated a hydraulically required grain size controlling the stability for each location, representing a broad proxy for the maximum grain size that should be mobilised under the observed hydraulic conditions.

3.4 Zone-wise bar analysis

We conducted a zone-wise (e.g., crest, middle, and tail) comparative analysis of multiple metrics to quantitatively assess the interplay between hydraulic, topographic, and

https://doi.org/10.5194/egusphere-2025-5145
Preprint. Discussion started: 28 October 2025

sedimentological factors across the bar morphology in Bar 3. For each zone, we compiled the absolute median values of key parameters derived from earlier methodological steps, including shear stress, Shields parameter, bed slope, surface elevation, relative elevation difference, and the local stability. To enable direct comparison between the parameters of differing units and scales, we normalised each metric by subtracting its minimum value and dividing by its range across the entire dataset, resulting in values scaled between 0 and 1. This normalisation ensured that all variables contributed equally to the zone-wise comparison, regardless of their actual magnitude or measurement units (Liu et al., 2025; Moreira et al., 2021; Saisana & Saltelli, 2011).

This approach enables us to compare and visualise the median, variability, and distribution of each parameter across bar zones. By integrating hydraulic, geomorphic, and stability metrics into a unified, zone-based framework, we assessed the interactions and relative controls that dictate bar-scale sediment responses to a 2-10-year return period flood. Specifically, we evaluated which physical factors most strongly influence sediment mobility and morphological change across different parts of the gravel bar.

3.5 Hydrological and climate trend analysis

To discuss the discharge regime of the Sense in light of our results, we applied a Gumbel distribution fit to the annual peak discharge series, following established methods for hydrological frequency analysis (Gumbel, 1942). This approach enabled us to estimate the return period and exceedance probability for key discharge values, including the 2023 flood of interest at 180 m^3/s. We further used the fitted distribution to derive the expected magnitude of rare events, such as the 100-year flood, and to calculate associated 95% confidence intervals for each estimated discharge resulting in the mobility of grains. This probabilistic analysis provides a robust statistical framework for interpreting both the severity and geomorphic significance of the observed high-flow events in the River Sense (Stedinger et al., 1993).

Finally, we performed a detailed analysis of the River Sense hydrological record to discuss the evolution of the flood regime and investigate trends in flood recurrence that may be related to climate. We first quantified the annual and decadal frequency of high-flow events by identifying exceedances of key discharge conditions required to mobilise the grains, specifically the 99th, 99.5th, and greater than 99.99th percentile values in the long-term hourly dataset. By aggregating event counts per decade, we evaluated the changing density of moderate and high-magnitude floods across the twentieth and early twenty-first centuries. We

https://doi.org/10.5194/egusphere-2025-5145
Preprint. Discussion started: 28 October 2025

applied least squares linear regression to estimate trends in the frequency of these events, highlighting shifts in the occurrence of moderate to moderately large floods over recent decades.

4 Results

4.1 Discharge scenario

To understand sediment redistribution in space and time as a function of hydrological regime, we need to consider the discharge regime of the River Sense because this sets the boundary conditions for sediment transport. Figure 2a presents the complete hourly discharge record for the River Sense from 1928 to 2025, highlighting the occurrence, frequency, and magnitude of flood events over nearly a century. There are some missing records between the years 1974 and 1977, which do not have any significant impact on this study. The blue-shaded region on Fig. 2a marks the interval between the two UAV-based field surveys, which took place on 30 September 2021 and 17 May 2024. The red dashed line denotes the 180 m³/s discharge, selected based on FOEN flood classification reports, which identify such events as having a return period of approximately 2-10 years for the River Sense. This discharge thus represents a moderately large flood, likely large enough to drive measurable sediment transport and morphological change, but not so rare as to be outside the range of expected natural variability.

The analysis of the discharge record confirms that the 14 November 2023 flood, which peaked at 185.5 m³/s, was the only event of this magnitude to occur between the 2021 and 2024 field campaigns (Fig. 2b). The flood exceeded the 180 m³/s discharge between 18:00 and 19:00, with flows remaining above 160 m³/s for at least four consecutive hours. We anticipate that this combination of peak discharge and event duration is more than sufficient to mobilise gravel and drive measurable morphological change, providing a well-documented opportunity to directly link sedimentary and topographic responses in the surveyed bars to a specific hydrological forcing.

4.2 Physical characteristics of sediment grain size

We measured a total of ca. 1.86 million gravel grains across two field surveys conducted in 2021 and 2024. Spatial distribution maps depicting the coarse sediment fraction (D84) from the 2024 survey clearly illustrate distinct sedimentary trends both within and among the surveyed gravel bars (Fig. 4a-d). In Fig. 4, the bars are presented in the following sequence:

https://doi.org/10.5194/egusphere-2025-5145
Preprint. Discussion started: 28 October 2025

Bar 1 (Fig. 4a), Bar 2 (Fig. 4b), Bar 3 (Fig. 4c), and Bar 4 (Fig. 4d). While Bar 1 is the most downstream site and Bar 4 the most upstream, Bars 2 and 3 are located at intermediate positions along the river. Each tile in these maps represents D84 grain size measurements averaged at a spatial resolution of 5 m².

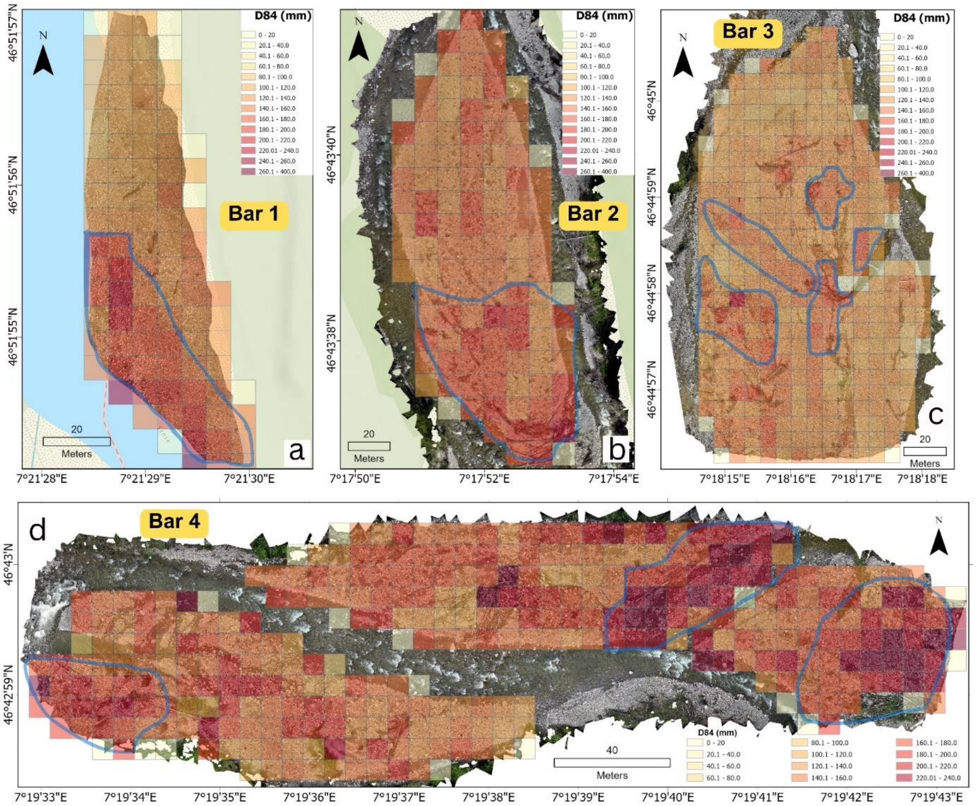

Figure 4: Spatial patterns of coarse fraction (D84) for Bars 1-4 (2024 survey). (a-d) Tile-based D84 (mm) mapped at 5 m² scale for Bar 1 (a), Bar 2 (b), Bar 3 (c), and Bar 4 (d). Blue polygons mark the coarse-grained patches in the grain-size distribution maps, which are interpreted to be mostly aligned with the historical channel traces and crest parts of the bar.

A clear intra-bar grain-size fining trend within each bar is recognisable, characterised by relatively coarse sediments dominating bar crests and progressively finer sediments towards the bar tails. This internal fining gradient is consistent across all surveyed bars, demonstrating systematic intra-bar downstream fining. Moreover, spatial patterns of D84 vividly display past signatures such as former channel alignments and paleo-bar crests. For instance, Bar 3 and Bar 4 show coarser grain sizes aligning closely with historical channel positions, indicative of

https://doi.org/10.5194/egusphere-2025-5145
Preprint. Discussion started: 28 October 2025

lag deposition processes associated with past fluvial configurations (blue polygons in Fig. 4c, d).

The cumulative distribution functions (CDFs) further clarify spatial and temporal sedimentological characteristics of each bar (Fig. 5). Panels within the green box (left) present grain size distributions from the 2024 survey (Fig. 5a, c, e, and g), while panels within the purple box (right) depict distributions from the 2021 survey (Fig. 6i, k, m, and o). Median grain sizes (D50) ranged from 75 mm to 90 mm in 2024, showing greater variability compared to the narrower range of 72 to 77 mm observed in 2021. Similarly, the coarser fraction (D84) exhibited a broader range in 2024 (130 mm to 174 mm) than in 2021 (122 mm to 134 mm). Furthermore, when the grain size distributions from all bars are normalised using the self-similar grain-size variable proposed by Fedele and Paola (2007), all individual bar curves collapse into a coherent and unified self-similar distribution (Fig. 5b, d, f, h, j, l, n, p). This convergence robustly supports the applicability of self-similarity concepts to sediment sorting processes observed in natural fluvial environments (e.g., Brooke et al., 2018; D'Arcy et al., 2017; Fedele & Paola, 2007). Despite local sedimentary variations, the consistent self-similar pattern across all studied bars highlights universal grain-sorting mechanisms dominating the river system.

In addition to these general patterns, a clear relationship between bar location within the reach and sorting emerges. Bar 4, in the relatively straight upstream reach, consistently displays poor sorting, with a broad cumulative curve and large separation between D50 and D84 (Fig. 5g, o). By contrast, Bars 1, 2, and 3, located in more sinuous reaches (Fig. 1a), show relatively steeper CDFs and narrower percentile spreads, indicating moderate to well-sorted sediments. This distinction suggests that local channel morphology exerts a strong influence on sorting efficiency, with straight reaches apparently favouring greater heterogeneity in surface textures compared to bends (see also do Prado et al., 2025a).

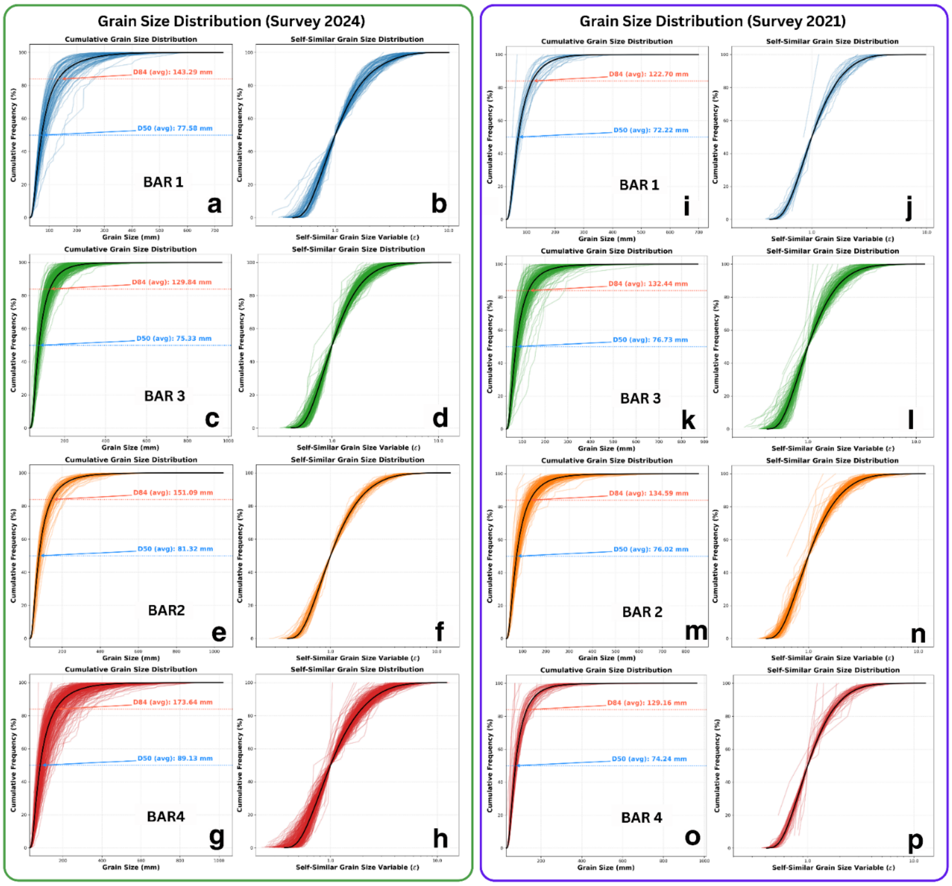

Figure 5: Grain-size distributions and self-similar grain size variable. Left column (green frames): Cumulative Distribution Functions (CDFs) of D50 and D84 for Bars 1-4 from the 2024 survey (a, c, e, g). Right column (purple frames): corresponding CDFs from the 2021 survey (i, k, m, o). Middle columns show the same data normalised with the self-similar grain-size variable (Fedele & Paola, 2007), which is calculated as in Fedele and Paola (2007). Consequently, the results demonstrate convergence towards a self-similar grain size form across sites and surveys (b, d, f, h, j, l, n, p).

Notably, the 2024 survey demonstrated a clear downstream fining trend in sediment grain size (Fig. 6a). Moving downstream in location from Bar 4 (upstream) to Bar 3 (midstream), both D50 and D84 decreased systematically from approximately 89 mm to 75 mm (D50) and from 173 mm to 129 mm (D84). However, at the original position of the downstream-most bar (Bar 1), sediments became relatively coarser again (D50 and D84: ca. 78 and 143 mm). In contrast, the 2021 survey exhibited a much less pronounced spatial gradient in grain-size distribution across the bars, with D50 and D84 values remaining relatively consistent between sites and

https://doi.org/10.5194/egusphere-2025-5145
Preprint. Discussion started: 28 October 2025

lacking a significant downstream fining pattern. Additionally, the overall distributions of both D50 and D84 appeared slightly coarser in the 2024 survey compared to those observed in late 2021, indicating a subtle shift towards coarser sediment fractions following the flood event. However, the geomorphic impacts of the November 14, 2023, flood event led to significant reconfiguration and migration of several gravel bars. For example, Bar 4 was almost entirely displaced from its original position and replaced by a new channel path (Fig. 6b, c), while others, such as Bar 1, experienced partial destruction or substantial lateral movement.

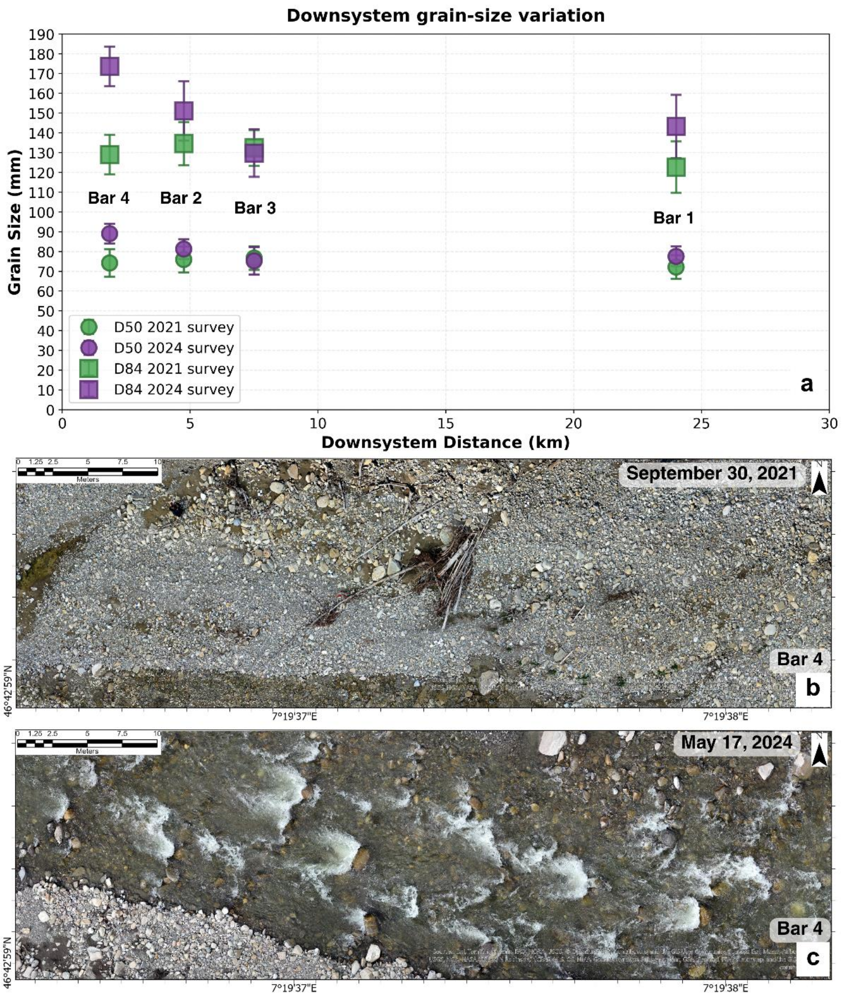

Figure 6: (a) Grain-size (D50 and D84) as a function of downsystem distance from the headwaters of the Sense River, where the green circle and square denote the D50 and D84 observed in the 2021 survey and the purple circle and square denote the D50 and D84 observed in the 2024 survey. Error bars represent a 95% confidence interval; (b-c) Example of the interpreted geomorphological impact of a moderately large flood (November 14, 2023)

https://doi.org/10.5194/egusphere-2025-5145
Preprint. Discussion started: 28 October 2025

that occurred between the two surveys, where part of Bar 4 has been completely reworked or destroyed, and the channel has shifted.

4.3 Sensitivity of grain-size distribution to floods

As the November 14, 2023 flood is by some margin the largest event to have affected the Sense River during the monitoring period and because it was associated with a marked geomorphic impact (above), we use this as a context to understand the sensitivity of grain size distributions to floods of this type. For our temporal analysis, we specifically focused on Bar 3. This bar provided the greatest spatial and temporal overlap between the two surveys, making it suited for high-resolution change detection. In contrast, at the other surveyed bars, the flood event caused extensive sediment mobilisation and large-scale positional shifts, such that only a limited area remained spatially consistent between both surveys. Figure 7 summarises how sediment grain-size distributions differed during the monitoring period, including the 14 November 2023 flood event at this bar, integrating spatial mapping, frequency distributions, and zone-wise statistical analysis (see also the supplement, Fig. S1 and S2).

In Fig. 7a and 7b, we mapped the D84 (the coarse fraction) across Bar 3 between surveys, with the crest, middle, and tail zones clearly delineated. While at the whole bar scale, the differences between the surveys for Bar 3 are relatively small compared to the other bars in this study, which were mostly or completely reworked (Fig. 6), our data give detailed insights into sediment mobilisation during the time period between the two surveys. In the first survey (Fig. 7a), we observed relatively coarse sediments concentrated in the tail of the bar (dark red colours). During the second survey (Fig. 7b), we detected a marked fining of the tail zone; D84 values dropped substantially, while the crest remained comparatively unchanged. The spatial map of absolute change (Fig. 7c) highlights that the most significant grain-size adjustments occurred in the middle and tail zones. A categorical view (Fig. 7d) shows fining was concentrated in the tail and adjacent transition zones, with localised coarsening mainly along crest-to-middle transitions. We then analysed the distribution of D84 values during two surveys (Fig. 7e and 7f), finding that the bar surface experienced variable adjustments in grain size, with many areas showing moderate changes in D84 and some zones undergoing much larger shifts (Fig. 7c and 7g), as supported by the coarsening and fining histogram (Fig. 7h).

To assess zonewise patterns, we compared absolute changes in D50 and D84 for the crest, middle, and tail (Fig. 7i). Changes in D50 are small in all zones (typically <10 mm), whereas D84 changes are larger and most variable in the tail (e.g., reaching beyond 100 mm). This pattern indicates that the flood event was able to mobilise coarser grains, particularly in the more hydraulically active, downstream portions of the bar.

https://doi.org/10.5194/egusphere-2025-5145
Preprint. Discussion started: 28 October 2025

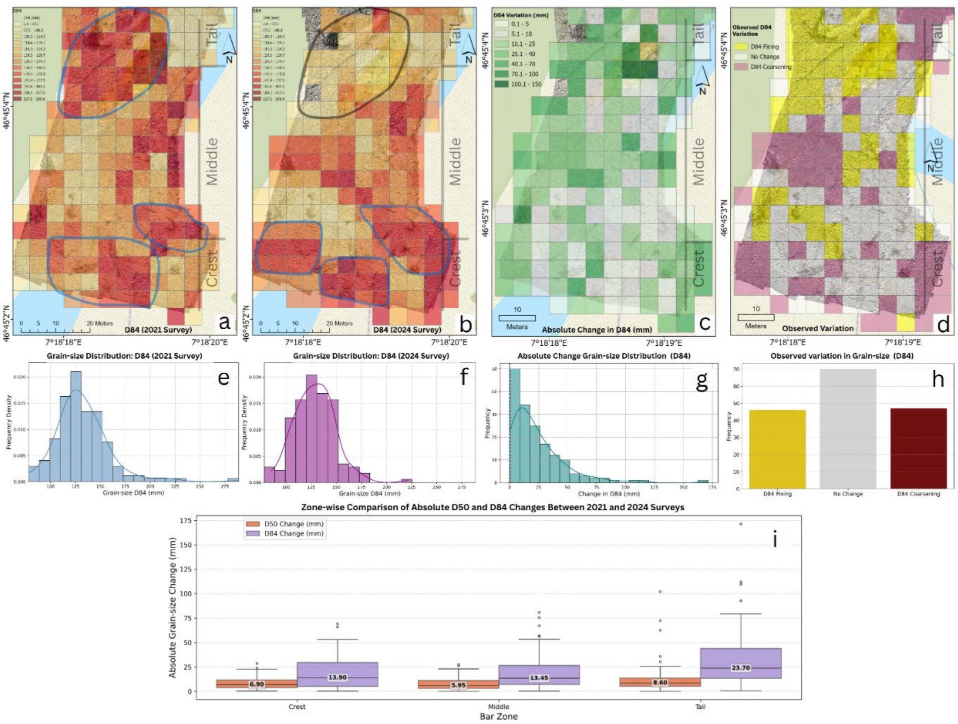

Figure 7: Grain-size variation between two surveys (2021, and 2024). Panels (a)-(b) show spatial D84 maps for the part of bar 3 between the surveys, where (c) illustrates the absolute change in D84, with darker greens reflecting larger magnitudes of change and white cells representing no significant variation. d) shows the observed categorical variation in D84, where yellow indicates fining, purple denotes coarsening, and light grey represents no significant change. Panels (e)-(f) present the frequency density of D84 from the two surveys, while panel (g) shows the frequency distribution of the absolute changes in D84 and panel. Panel (h) summarises fining and coarsening in a histogram, using consistent colour coding (yellow for fining, purple for coarsening, and light grey for no change). Panel (i) quantifies absolute changes in D50 and D84 by morphological zone (crest, middle, tail).

4.4 Hydraulic parameters and sediment mobility

Spatial analysis of the hydraulic parameters calculated from high-resolution digital surface models (DSMs) extracted from both surveys demonstrates clear and distinctive hydraulic conditions across the studied gravel bar (Fig. 8). The relative elevation change (Fig. 8a), derived by differencing DSMs captured before and after the flood event, indicates that deposition dominated across Bar 3 (green tiles). To account for potential survey uncertainties, changes within ±0.06 m were classified as “no detectable change”, ensuring that only shifts beyond this threshold were interpreted as geomorphically significant. The frequency

https://doi.org/10.5194/egusphere-2025-5145
Preprint. Discussion started: 28 October 2025

distribution (Fig. 8e) reflects this filtering; for example, the plot is mostly right-skewed, with the most values falling in the depositional range of 0.06-0.5 m. Although local erosion has occurred near the edges, it was spatially restricted and significantly less extensive compared to the depositional areas.

To better understand the drivers of these depositional patterns, we analysed the spatial distribution of bed shear stress associated with the 2023 flood event (Fig. 8b), based on hydraulic modelling (see Methods). Calculated shear stress values exhibited significant spatial variability across the bar (Fig. 8b), with lower modelled shear stress values prevalent in the elevated crest region, generally remaining below 140 Pa, whereas modelled shear stress exceeded 650 Pa in several areas along the bar tail, correlating well with observed zones of intense sediment mobilisation. The frequency distribution (Fig. 8f) reflects this, with the majority of calculated shear stress falling within the range of 1 to 200 Pa. From the calculated shear stress, critical Shields stress, observed median grain size and water depth, sediment entrainment predictions were modelled spatially (Fig. 8c). Our model results predict that sediment mobilisation primarily would occur across the middle and tail portions of the bar, with high degrees of spatial complexity (red tiles, Fig. 8c). The Shields parameter distribution (Fig. 8g) shows that most values remained below 0.2, but a substantial tail of higher values concentrated in the bar tail matched observed mobilisation. These model predictions aligned reasonably well with the observed mobilisation patterns derived from absolute D84 grain-size changes, achieving approximately 65% accuracy overall. Spatial accuracy varied significantly: the bar tail showed excellent prediction alignment (82%), reflecting well-captured hydraulic thresholds and grain mobility conditions; the middle region predictions showed intermediate accuracy (64%), while predictions for the crest region were notably lower (42%). Here, observed mobility exceeded modelled predictions, particularly near the bar edges around the crest, where our simple hydraulic threshold approach did not anticipate sediment movement. This difference suggests that, in these locations, factors such as local topography and proximity to active channel thalweg may facilitate sediment mobilisation from the bar even under apparently sub-threshold conditions.

Further, spatial mapping of the stability condition grain size (Fig. 8d) estimated the critical D50 required for sediment immobility under modelled hydraulic conditions. Stability conditions exhibited considerable variability, which is also reflected in the frequency diagram (Fig. 9h), with grain sizes exceeding 350 mm required in many parts of the tail zone to maintain sediment immobility. In contrast, the crest required smaller grain sizes (<90 mm) for stability, aligning with observed sediment stability and minimal grain-size change.

https://doi.org/10.5194/egusphere-2025-5145
Preprint. Discussion started: 28 October 2025

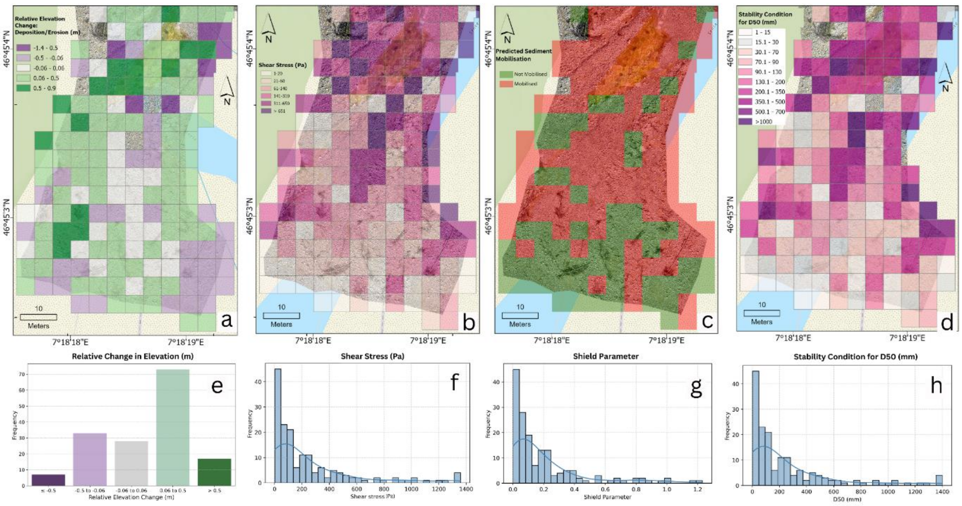

Figure 8: Observed changes across Bar 3 between the two surveys and hydraulic controls on observed mobility. (a) shows the relative change in elevation between two surveys (green = net deposition; purple = erosion, with changes within ±6 cm considered not significant to account for potential survey uncertainties), (b) shows the spatial distribution of calculated bed shear stress, (c) Predicted sediment mobilisation based on local Shields exceedance, where green indicates no mobilisation and red highlights areas of higher mobilisation likelihood, particularly clustering in the middle and tail zones; (d) shows an estimated grain size stability condition (D50) map based on the predicted sediment mobilisation. (e) Frequency distribution of relative elevation change, corresponding to the classes defined in panel (a); Panels (f), (g), and (h) show the frequency distribution of relative change in elevation, shear stress, shield parameter, and stability condition median grain size, respectively.

Figure 9 synthesises the key topographic and hydraulic controls on bar-scale sediment adjustment by presenting metrics in a normalised (0-1) form for direct zone-wise comparison. Elevation is highest in the crest (median = 0.81), decreases through the middle (0.56), and reaches its lowest values at the tail (0.25), reflecting the overall downstream bar morphology. Relative elevation difference, by contrast, remains consistently high across all zones, with medians between 0.61 and 0.67. This uniformity indicates that the flood event eventually promoted net aggradation rather than widespread erosion for this bar, with all zones maintaining or slightly increasing their relative elevation compared to local surroundings. While sediment could be mobilised from the bar at the flood peak, this was more than balanced by deposition integrated over the course of the flood.

https://doi.org/10.5194/egusphere-2025-5145
Preprint. Discussion started: 28 October 2025

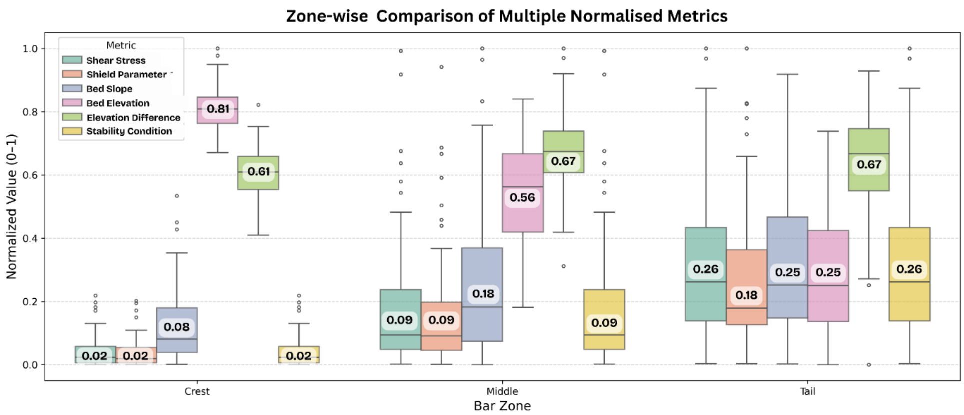

Figure 9: Zone-wise comparison of topographic and hydraulic drivers (normalised). Normalised (0-1) median values for elevation (pink), relative elevation change (light green), bed slope (grey), shear stress (dark green), Shields parameter (orange), and grain-size stability condition (yellow) across crest, middle, and tail zones of Bar 3. This integrates heterogeneous metrics on a common scale and highlights the co-increase of slope, stress, Shields, and stability condition toward the bar tail relative to the crest.

Zone-wise normalised hydraulic metrics show a systematic downstream increase. Median shear stress is very low in the crest (0.02), rises in the middle (0.09), and peaks at the tail (0.26). The Shields parameter follows a similar pattern, with medians of 0.02, 0.09, and 0.18 for crest, middle, and tail, respectively. Bed slope also steepens progressively, from 0.08 at the crest to 0.18 in the middle and 0.25 at the tail. The stability condition, which reflects a minimum grain size predicted to be mobilised under flood conditions, shows the same trend, increasing from 0.02 in the crest to 0.09 in the middle and 0.26 in the tail.

Together, these patterns illustrate a clear differentiation of bar zones: the crest, though topographically highest, remained relatively stable due to low hydraulic forcing; the middle experienced intermediate levels of reworking; and the tail was the most dynamic zone, where the convergence of steep slopes and high stresses promoted widespread grain mobilisation and redistribution.

5 Discussion

5.1 UAV and machine learning for grain size characterisation

Our study underlines the capability of UAV-based photogrammetry, when combined with machine-learning-driven grain-size measurement, to resolve spatial and temporal

https://doi.org/10.5194/egusphere-2025-5145
Preprint. Discussion started: 28 October 2025

sedimentary dynamics at a high resolution. The resulting high-density, spatially explicit dataset enables robust quantification of sediment redistribution and sorting and facilitates empirical tests of self-similar organisation frameworks that directly link sediment mobilisation to hydrological dynamics (Fedele & Paola, 2007). While traditional methods, including direct field sampling, Wolman pebble counting, and manual sediment mapping, have provided fundamental insights into river dynamics, they can be spatially limited, time-intensive, and labour-intensive (Buffington & Montgomery, 2013; Bunte & Abt, 2001; Rice & Church, 2010; M. G. Wolman, 1954). The integration of machine learning algorithms with UAV-based imagery, exemplified here, enhances this methodological framework by automating grain segmentation and measurement, achieving reliable results at centimetre scale (Chen et al., 2022; Mair et al., 2024; Miazza et al., 2024).

A further strength of our approach lies in the use of area-by-number grain-size statistics calculated in fixed 5 m × 5 m tiles (principal axes a and b in mm), which provide dense and internally consistent samples suited to detecting surface variation, patch boundaries, and partial-transport responses (Bunte & Abt, 2001; Mair et al., 2022). Our approach provides robust empirical validation of self-similarity-based fining and demonstrates the applicability of dimensionless grain-size distribution frameworks in modern fluvial environments in a data set of > 1.8 million grains (Brooke et al., 2018; D'Arcy et al., 2017; Fedele & Paola, 2007). The scale of analysis also offers insights into grain-size sorting; for example, poorly sorted sediments in the straight upstream reaches of the Sense river and better-sorted material in bend-associated bars (see Fig. 5) support established fluvial theory (Clayton, 2010), showing that morphological control on sorting persists in braided gravel-bed systems as well as in meandering rivers.

Recent roughness-based studies suggest that surface texture patterns of grain-size distribution can preserve hydrological imprints at reach scale (e.g., Ribet et al., 2025). Here, in this work, grain-level segmentation complements these broader approaches by providing detailed, clast-level quantification of grain-size distribution, remobilisation, and sediment patch heterogeneity, allowing explicit assessment of localised sediment heterogeneity and grain mobility patterns, which are challenging to resolve through roughness proxies alone. Importantly, the robustness of this approach is enhanced by using the default segmentation model of ImageGrains, which was, among other data, trained and validated on Sense River imagery (see S1 in Mair et al., 2024), ensuring the detection quality is well-adapted to the geomorphic characteristics of the study site. Consequently, the approach developed here offers scalability and applicability across diverse geomorphic contexts, with the potential to markedly enhance river monitoring in response to floods, sediment budgeting, and predictive modelling for both scientific research and practical river management.

https://doi.org/10.5194/egusphere-2025-5145
Preprint. Discussion started: 28 October 2025

5.2 Linking hydraulic conditions with sediment mobility

Our high-resolution spatial analysis of grain-size distributions in the Sense River demonstrates clear and detailed relationships between sediment mobility and local hydraulic conditions, particularly during moderately large flood events. Distinct intra-bar grain-size patterns and downstream fining, alongside well-defined patch-scale variability, emphasise the importance of hydraulic heterogeneity in governing sediment transport dynamics (Ashworth et al., 2000; Bridge & Best, 1988; Wilcock & Crowe, 2003).

High-resolution relative elevation-change mapping (Fig. 8a, e) indicates net deposition-dominated dynamics during the moderately large flood event for the studied bar (Bar 3). These results illustrate how moderately large floods can also serve as sediment-delivery mechanisms rather than as purely erosive agents, significantly reshaping bar morphology via depositional processes (Ashworth et al., 2000; Nicholas, 2013). Notably, substantial sediment rearrangement can occur even where median grain-size values appear relatively stable, highlighting the complexity of sediment transport and the occurrence of significant particle exchange and surface reworking processes that do not necessarily alter overall grain-size metrics. This can be interpreted in the context of the flood hydrograph; for example, this pattern reflects selective mobilisation during peak flow, followed by widespread deposition and surface renewal during the waning stage, yielding a depositional blanket that preserves overall bar relief while recording marked intra-bar reworking (Bridge & Best, 1988; Venditti et al., 2012).

The spatial distribution of hydraulic parameters (Fig. 8 and Fig. 9) further clarifies mechanisms of patch-scale sediment mobilisation during moderate floods. Crest zones in all four bars (Fig. 4) predominantly retain coarse grains due to their hydraulically elevated positions, resulting in stable lag deposits and coarse-grained patches. These stable surfaces, or armours, resist mobilisation during moderate hydraulic forcing because of lower shear stress (Church & Hassan, 1992; Dietrich et al., 1989; do Prado et al., 2025a; Wilcock & McArdell, 1993), as confirmed by shear stress mapping of Bar 3 (Fig. 8b). In contrast, bar tails experience selective deposition of finer sediments, likely driven by flow deceleration. These observed downstream fining patterns within individual bars strongly align with established sediment sorting theories linked to spatial gradients in shear stress and hydraulic energy (Ashworth et al., 2000; Bridge & Best, 1988).

Finally, while roughness-based mapping can capture reach-scale textural patterns and hydrological imprints (Ribet et al., 2025), our grain-resolved approach adds what those proxies cannot; for example, in this study, we explicitly linked the continuously mapped grain-size

https://doi.org/10.5194/egusphere-2025-5145
Preprint. Discussion started: 28 October 2025

patchiness with sediment mobilisation mechanisms through detailed hydraulic modelling (e.g., shear stress and shield parameter), which bridges the classical sedimentological theory with modern high-resolution mapping techniques (Fig. 8-9). Recent work on the Sense River by do Prado et al. (2025a) highlights the geomorphic importance of sedimentological architecture, particularly the preservation potential of lateral lag deposits along bar margins. Our results support and extend these findings by demonstrating that lag deposits along bar crests and edges influence bar stability, preserving historical sedimentary structures. For example, Bar 4 retains clear sedimentary imprints of coarse-grained bar margins (blue polygons, Fig. 4). However, we also observe that local hydraulic geometry can override patch-scale effects; for example, in the steep-sloped tail zone of Bar 3 (Fig. 7a, b, c), coarse patches (blue polygon in the tail part of Fig. 8a) can be rapidly buried or replaced by new deposits, causing coarse patches to transition into relatively fine-patch layers, where high shear stress and mobility thresholds are exceeded (black polygon in Fig. 8b). Similarly, these hydrological conditions have also led to complete erosion or destruction of sub-bar features (Fig. 6b). These observations show that sediment preservation versus erosion reflects a complex interplay of multiple interacting factors, including hydraulic energy distribution, bar morphology, local slope conditions, and grain-size distributions, rather than a single controlling factor.

Our comparative normalised magnitude-based analysis of hydraulic parameters, including bed slope, elevation, shear stress, Shields parameter, relative elevation differences between surveys, and stability condition, clarifies the functional links between hydraulic conditions and sediment mobility (Fig. 9). Elevation decreases systematically from crest to tail, defining a classic downstream gradient in bar morphology, while relative elevation differences between two surveys remain nearly constant between zones. This uniform distribution of material is consistent with waning-stage deposition that raised surfaces without altering inter-zone relief. Importantly, the along-bar gradients in slope, shear stress, and Shields parameter explain the observed grain-size adjustments; crests remain relatively immobile, whereas mobility increases downstream, with middle zones showing moderate rearrangement and tails experiencing the most active reworking (cf. Buffington & Montgomery, 1997; Wilcock & Crowe, 2003).

5.3 Potential influence of climate change on gravel-river morphodynamics

The long-term hydrological records from the Sense River (FOEN, 2025) provide direct insight into flood magnitude-frequency relationships and their evolving temporal characteristics (Fig. 10a). The flood event analysed in this study, with a peak discharge of approximately 180 m³/s,

https://doi.org/10.5194/egusphere-2025-5145
Preprint. Discussion started: 28 October 2025

is described by the FOEN as representing a 2-10-year event. Our analysis demonstrates that it corresponds to a specific return period of 5.7 years (annual exceedance probability ca. 20%) analysing across all data from 1928 to the present day (Fig. 10a). By comparison, rare extreme floods, such as the 100-year event (ca. 290 m³/s), provide the highest extent to which the high-magnitude geomorphic change can take place (Lane et al., 2017). However, due to their low frequency, these large floods may play a less dominant role in the incremental geomorphic adjustments typically observed over decadal scales. Our results, therefore, may suggest that cumulative morphological adjustments are driven by the more frequent, moderate- to moderately large magnitude events. This interpretation is consistent with the Alpine precipitation scaling reported by Molnar & Burlando (2008), who argued that short-duration, convective summer precipitation dominates high-frequency variability and intermittency conditions that can preferentially generate moderate, geomorphically effective floods even without concurrent rises in the most extreme discharges.

This finding aligns with the known sensitivity of the gravel-bed rivers, especially in alpine basins, to the shifts in hydrological regime, where runoff is governed by a mix of snowmelt, rain-on-snow, and short-duration convective storms. Morphology, sediment transport dynamics, and associated ecological habitats depend closely on local hydrological regimes, making these systems particularly sensitive to climate change-induced hydrological alterations (Beniston et al., 2018; Blöschl et al., 2019; Lobanova et al., 2018; O'Briain, 2019). Climate projections consistently predict substantial shifts in precipitation patterns, including increased frequency and intensity of extreme rainfall events, alongside altered snowmelt dynamics in mountainous regions such as the Swiss Alps (Blöschl et al., 2019; Lane et al., 2017). These changes are expected to fundamentally modify flood regimes, sediment transport thresholds, and channel morphology through the twenty-first century.

Our analysis of the gauging data in Fig. 10b suggests a clear trend towards increased frequency of moderate magnitude flood events (50-65 m³/s) over recent decades, a trend that might be expected to intensify through 2030 and beyond (Birsan et al., 2005; Glur et al., 2013). In contrast, the frequency of larger floods (≥180 m³/s) has not yet shown significant changes. This pattern of more frequent moderate flows without a clear rise in the most extreme discharge events is consistent with regional observations across Central Europe and Switzerland, where earlier spring snowmelt, declining seasonal snow storage, and more intense short-duration rainfall increase runoff and rain-on-snow contributions (Beniston et al., 2018; Blöschl et al., 2019; Kundzewicz et al., 2017). In snow-influenced basins such as the Sense, this could translate into (i) higher frequency of moderate peaks superimposed on the melt hydrograph (see Fig. S3 for discharge seasonality) and (ii) potential episodic summer-autumn spikes from convective rainfall.

https://doi.org/10.5194/egusphere-2025-5145
Preprint. Discussion started: 28 October 2025

From a geomorphological perspective, an increasing frequency of moderate to moderately large flood events has important implications for river sediment dynamics. Our results show that even events of moderately large magnitude can mobilise significant areas in the bars studied here, particularly where sediment mobility conditions are most readily exceeded (see Fig. 8), in some cases, resulting in the removal of entire sub-bar units (Fig. 6b). Increased sediment turnover and frequent reworking during moderate events may therefore lead to significant morphological dynamism and altered sediment sorting patterns. Consequently, by 2100, gravel-bed rivers in the Alps, such as the Sense, could experience significant morphological transformations; for instance, bars may become more transient, dynamically responding to frequent disturbances, potentially shifting river planforms toward less stable configurations, including more active braiding-dominated regimes (Lane et al., 2017; Slater et al., 2017). Such morphological transitions could significantly impact riverine ecosystems, altering habitat diversity, availability, and ecological connectivity and posing challenges for sustainable river management. Further work to evaluate sediment and bar mobility in these rivers will be important to understand these changes. Consequently, we advocate integrated approaches that combine high-resolution geomorphological monitoring, hydrological modelling, and climate projections to manage climate-influenced changes in fluvial dynamics.

https://doi.org/10.5194/egusphere-2025-5145
Preprint. Discussion started: 28 October 2025

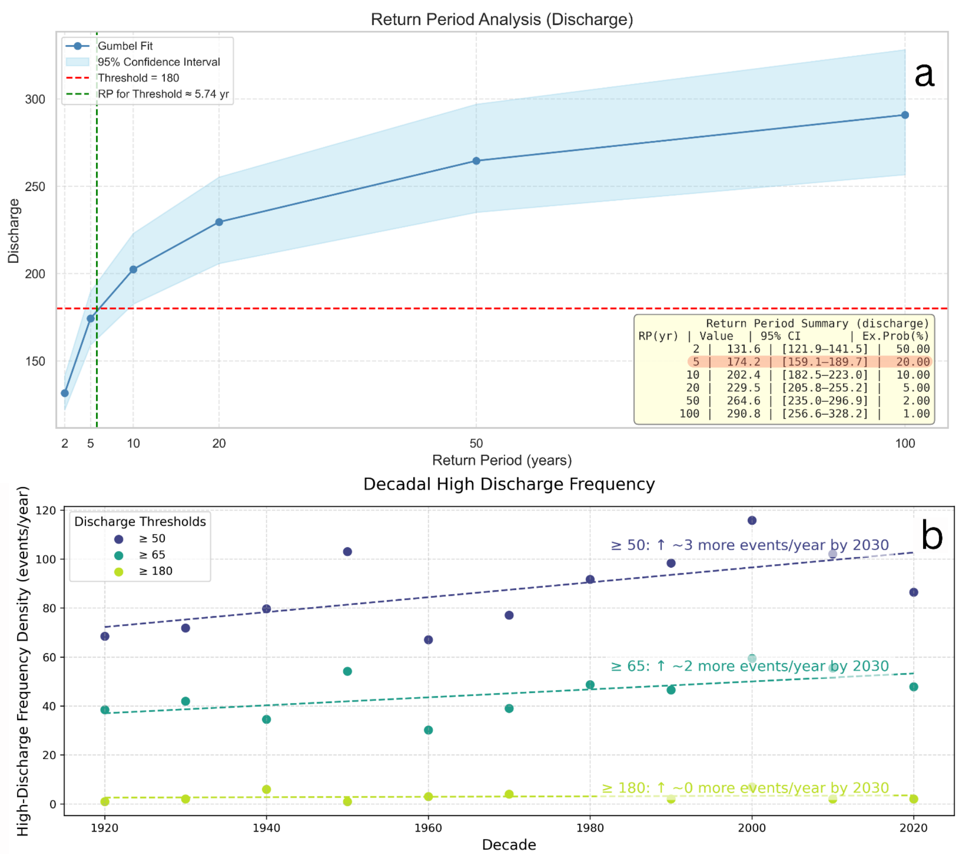

Figure 10: Flood-frequency context for the Sense River based on gauging data from 1920 to present (FOEN, 2025). (a) shows the return period and exceedance probability analysis for annual peak discharges, based on a Gumbel distribution fit. We mark the threshold used in this study with a red horizontal dashed line (180 m³/s flood). Panel (b) highlights the decadal event density for moderate and high discharge thresholds (the 99th, 99.5th and 99.99th percentiles are presented as blue, green and yellow dots with matching coloured dashed trend lines indicating multi-decadal changes in the density). This data suggests a clear increase in moderate-sized events is already present in the Sense over the last century.

6 Conclusions

This study provides a detailed, grain-to-bar scale perspective on how a minimally disturbed gravel-bed river responds to a moderately large flood event, using the River Sense as a case study. By combining UAV-based structure-from-motion photogrammetry with machine-learning-driven grain-size analysis, we were able to quantify sediment redistribution at an unprecedented resolution, tracing and measuring approximately 1.86 million individual grains.

https://doi.org/10.5194/egusphere-2025-5145
Preprint. Discussion started: 28 October 2025

This level of detail not only captures the fine-scale spatial organisation of sediment but also enables explicit linkage between grain mobility, local hydraulic conditions, and broader morphological change.

Morphological setting also influenced sorting: the straight upstream reach (Bar 4) exhibited poorer sorting and wider percentile spreads, while bars located in bends (Bars 1–3) displayed moderate to well sorting, reflecting the interaction between flow curvature, sediment sorting, and bar morphology. Grain-size distributions retain self-similar scaling through these adjustments, providing rare empirical validation of scale-invariant sediment organisation across a full bar system.

To examine how these sorting patterns respond to hydrological forcing at grain scale, we conducted a detailed hydraulic-sediment analysis on part of Bar 3 capturing the November 2023 flood (ca. 180 m^3/s; 5.7-year recurrence), the most significant event between our two surveys in late 2021 and mid-2024. This grain-scale focus demonstrated how flood-driven spatial gradients in shear stress, Shields parameter, slope, and stability thresholds governed sediment redistribution. Crest zones, with low shear and gentle slopes, persisted as stable deposits, while steeply sloped tails experienced the greatest reworking. Importantly, local hydraulic geometry could override patch stability, with coarse fractions buried or entirely replaced where mobility thresholds were exceeded.

Long-term hydrological records show that moderate floods, below historical extremes (<200 m^3/s), can remobilise extensive bar areas and even remove entire sub-bar units. These floods are projected to become more frequent, suggesting that cumulative morphological change in the coming decades will be driven primarily by recurrent moderate events rather than rare extremes, promoting bar transience, shortening surface residence times, and shifting planforms toward more active braiding by the end of the century.

By bridging classical sedimentology with grain-resolved remote sensing, this research demonstrates the fine-scale processes through which moderate to moderately large floods drive morphological change in gravel-bed rivers. The methodological framework developed here for continuous, high-resolution mapping of sediment sorting, patch stability, and hydraulic thresholds offers a transferable toolset for decoding geomorphic responses under non-stationary hydrology. In practical terms, it highlights the need for river management strategies that focus not only on rare design floods but also on the moderate to moderately large, more frequent flows that quietly yet persistently reshape these dynamic systems in a changing climate.

https://doi.org/10.5194/egusphere-2025-5145
Preprint. Discussion started: 28 October 2025

Data availability

The dataset used in this study is available at Zenodo: https://doi.org/10.5281/zenodo.17370306

Author contributions

NR designed the study, processed and analysed all datasets, implemented the analytical workflows, prepared the figures, and wrote the original manuscript. DM, ACW, and FS contributed to the conceptualisation of the study. DM also assisted with UAV data collection, data curation, software support, and manuscript review. ACW and FS supervised the research, provided scientific guidance and editorial feedback, and secured project funding through the Source-to-Sink Future ITN (Horizon 2020 Marie Skłodowska-Curie Actions, Grant Agreement No. 860383). AHdP contributed prior datasets from the same field sites and assisted in data curation and manuscript review. SHS provided technical input on data visualisation and assisted in reviewing the manuscript. All authors discussed the results and contributed to the final version of the paper.

Competing interests

The authors declare that they have no conflict of interest.

Acknowledgements

The authors thank the Institute of Geology, University of Bern, for hosting NR during his research secondment and for providing access to logistical support for UAV fieldwork and to computational facilities used for data processing. This research received funding from the European Union’s Horizon 2020 research and innovation programme under the Marie Skłodowska-Curie grant agreement No. 860383 (Source-to-Sink Future ITN).

https://doi.org/10.5194/egusphere-2025-5145
Preprint. Discussion started: 28 October 2025

7 References

Arnaud, F., Piégay, H., Schmitt, L., Rollet, A. J., Ferrier, V., & Béal, D. (2015). Historical geomorphic analysis (1932–2011) of a by-passed river reach in process-based restoration perspectives: The Old Rhine downstream of the Kembs diversion dam (France, Germany). *Geomorphology*, *236*, 163–177. https://doi.org/10.1016/j.geomorph.2015.02.009

Arnaud, F., Schmitt, L., Johnstone, K., Rollet, A.-J., & Piégay, H. (2019). Engineering impacts on the Upper Rhine channel and floodplain over two centuries. *Geomorphology*, *330*, 13–27. https://doi.org/10.1016/j.geomorph.2019.01.004

Ashmore, P. E., & Rennie, C. D. (2013). Gravel-bed rivers: From particles to patterns. *Earth Surface Processes and Landforms*, *38*(2), 217–220. https://doi.org/10.1002/esp.3361

Ashworth, P. J., Best, J. L., Roden, J. E., Bristow, C. S., & Klaassen, G. J. (2000). Morphological evolution and dynamics of a large, sand braid-bar, Jamuna River, Bangladesh. *Sedimentology*, *47*(3), 533–555. https://doi.org/10.1046/j.1365-3091.2000.00305.x

Ashworth, P. J., Ferguson, R. I., Ashmore, P. E., Paola, C., Powell, D. M., & Prestegaards, K. L. (1992). Measurements in a Braided River chute and lobe: 2. Sorting of bed load during entrainment, transport, and deposition. *Water Resources Research*, *28*(7), 1887–1896. https://doi.org/10.1029/92WR00702

Beechie, T. J., Sear, D. A., Olden, J. D., Pess, G. R., Buffington, J. M., Moir, H., Roni, P., & Pollock, M. M. (2010). Process-based Principles for Restoring River Ecosystems. *BioScience*, *60*(3), 209–222. https://doi.org/10.1525/bio.2010.60.3.7

Beniston, M., Farinotti, D., Stoffel, M., Andreassen, L. M., Coppola, E., Eckert, N., Fantini, A., Giacona, F., Hauck, C., Huss, M., Huwald, H., Lehning, M., López-Moreno, J.-I., Magnusson, J., Marty, C., Morán-Tejéda, E., Morin, S., Naaim, M., Provenzale, A., … Vincent, C. (2018). The European mountain cryosphere: A review of its current state, trends, and future challenges. *The Cryosphere*, *12*(2), 759–794. https://doi.org/10.5194/tc-12-759-2018

Bertoldi, W., Zanoni, L., & Tubino, M. (2010). Assessment of morphological changes induced by flow and flood pulses in a gravel bed braided river: The Tagliamento River (Italy). *Geomorphology*, *114*(3), 348–360. https://doi.org/10.1016/j.geomorph.2009.07.017

Birsan, M.-V., Molnar, P., Burlando, P., & Pfaundler, M. (2005). Streamflow trends in Switzerland. *Journal of Hydrology*, *314*(1–4), 312–329. https://doi.org/10.1016/j.jhydrol.2005.06.008

Blöschl, G., Hall, J., Viglione, A., Perdigão, R. A. P., Parajka, J., Merz, B., Lun, D., Arheimer, B., Aronica, G. T., Bilibashi, A., Boháč, M., Bonacci, O., Borga, M., Čanjevac, I.,

https://doi.org/10.5194/egusphere-2025-5145
Preprint. Discussion started: 28 October 2025

Castellarin, A., Chirico, G. B., Claps, P., Frolova, N., Ganora, D., … Živković, N. (2019). Changing climate both increases and decreases European river floods. *Nature*, *573*(7772), 108–111. https://doi.org/10.1038/s41586-019-1495-6

Bridge, J. S., & Best, J. L. (1988). Flow, sediment transport and bedform dynamics over the transition from dunes to upper-stage plane beds: Implications for the formation of planar laminae. *Sedimentology*, *35*(5), 753–763. https://doi.org/10.1111/j.1365-3091.1988.tb01249.x

Brierley, G., Fryirs, K., & Jain, V. (2006). Landscape connectivity: The geographic basis of geomorphic applications. *Area*, *38*(2), 165–174. https://doi.org/10.1111/j.1475-4762.2006.00671.x

Brooke, S. A. S., Whittaker, A. C., Armitage, J. J., D'Arcy, M., & Watkins, S. E. (2018). Quantifying Sediment Transport Dynamics on Alluvial Fans From Spatial and Temporal Changes in Grain Size, Death Valley, California. *Journal of Geophysical Research: Earth Surface*, *123*(8), 2039–2067. https://doi.org/10.1029/2018JF004622

Buffington, J. M., & Montgomery, D. R. (1997). A systematic analysis of eight decades of incipient motion studies, with special reference to gravel-bedded rivers. *Water Resources Research*, *33*(8), 1993–2029. https://doi.org/10.1029/96WR03190

Buffington, J. M., & Montgomery, D. R. (2013). 9.36 Geomorphic Classification of Rivers. In *Treatise on Geomorphology* (pp. 730–767). Elsevier. https://doi.org/10.1016/B978-0-12-374739-6.00263-3

Bunte, K., & Abt, S. R. (2001). Sampling Frame for Improving Pebble Count Accuracy in Coarse Gravel-Bed Streams. *JAWRA Journal of the American Water Resources Association*, *37*(4), 1001–1014. https://doi.org/10.1111/j.1752-1688.2001.tb05528.x

Buscombe, D. (2013). Transferable wavelet method for grain-size distribution from images of sediment surfaces and thin sections, and other natural granular patterns. *Sedimentology*, *60*(7), 1709–1732. https://doi.org/10.1111/sed.12049

Butler, J. B., Lane, S. N., & Chandler, J. H. (2001). Automated extraction of grain-size data from gravel surfaces using digital image processing. *Journal of Hydraulic Research*, *39*(5), 519–529. https://doi.org/10.1080/00221686.2001.9628276

Chen, X., Hassan, M. A., & Fu, X. (2022). Convolutional neural networks for image-based sediment detection applied to a large terrestrial and airborne dataset. *Earth Surface Dynamics*, *10*(2), 349–366. https://doi.org/10.5194/esurf-10-349-2022

Chessman, B. C., Fryirs, K. A., & Brierley, G. J. (2006). Linking geomorphic character, behaviour and condition to fluvial biodiversity: Implications for river management. *Aquatic Conservation: Marine and Freshwater Ecosystems*, *16*(3), 267–288. https://doi.org/10.1002/aqc.724

https://doi.org/10.5194/egusphere-2025-5145
Preprint. Discussion started: 28 October 2025

Church, M. (2002). Geomorphic thresholds in riverine landscapes. *Freshwater Biology*, *47*(4), 541–557. https://doi.org/10.1046/j.1365-2427.2002.00919.x

Church, M. (2006). BED MATERIAL TRANSPORT AND THE MORPHOLOGY OF ALLUVIAL RIVER CHANNELS. *Annual Review of Earth and Planetary Sciences*, *34*(1), 325–354. https://doi.org/10.1146/annurev.earth.33.092203.122721

Church, M., & Hassan, M. A. (1992). Size and distance of travel of unconstrained clasts on a streambed. *Water Resources Research*, *28*(1), 299–303. https://doi.org/10.1029/91WR02523

Clayton, J. A. (2010). Local sorting, bend curvature, and particle mobility in meandering gravel bed rivers. *Water Resources Research*, *46*(2), 2008WR007669. https://doi.org/10.1029/2008WR007669

D'Arcy, M., Whittaker, A. C., & Roda-Boluda, D. C. (2017). Measuring alluvial fan sensitivity to past climate changes using a self-similarity approach to grain-size fining, Death Valley, California. *Sedimentology*, *64*(2), 388–424. https://doi.org/10.1111/sed.12308

Dietrich, W. E., Kirchner, J. W., Ikeda, H., & Iseya, F. (1989). Sediment supply and the development of the coarse surface layer in gravel-bedded rivers. *Nature*, *340*(6230), 215–217. https://doi.org/10.1038/340215a0

Dingle, E. H., Sinclair, H. D., Venditti, J. G., Attal, M., Kinnaird, T. C., Creed, M., Quick, L., Nittrouer, J. A., & Gautam, D. (2020). Sediment dynamics across gravel-sand transitions: Implications for river stability and floodplain recycling. *Geology*, *48*(5), 468–472. https://doi.org/10.1130/G46909.1

do Prado, A., Galeazzi, C. P., Mair, D., Garefalakis, P., De Almeida, R. P., Whittaker, A. C., & Schlunegger, F. (2025a). Gravel bar shielding: A mechanism responsible for bar stability in gravel- and cobble-bedded streams. *Earth Surface Processes and Landforms*, *50*(7), e70107. https://doi.org/10.1002/esp.70107

do Prado, A. H., Mair, D., Garefalakis, P., Schmidt, C., Whittaker, A., Castelltort, S., & Schlunegger, F. (2024). Check dam impact on sediment loads: Example of the Guerbe River in the Swiss Alps – a catchment scale experiment. *Hydrology and Earth System Sciences*, *28*(5), 1173–1190. https://doi.org/10.5194/hess-28-1173-2024

do Prado, A. H., Mair, D., Garefalakis, P., Silveira, B. C., Whittaker, A. C., & Schlunegger, F. (2025b). The influence of grain size sorting on the roughness parametrization of gravel riverbeds. *Geomorphology*, *471*, 109565. https://doi.org/10.1016/j.geomorph.2024.109565

Efron, B., & Tibshirani, R. (1986). Bootstrap Methods for Standard Errors, Confidence Intervals, and Other Measures of Statistical Accuracy. *Statistical Science*, *1*(1), 54–75. JSTOR.

https://doi.org/10.5194/egusphere-2025-5145
Preprint. Discussion started: 28 October 2025

Eltner, A., Kaiser, A., Castillo, C., Rock, G., Neugirg, F., & Abellán, A. (2016). Image-based surface reconstruction in geomorphometry – merits, limits and developments. *Earth Surface Dynamics*, *4*(2), 359–389. https://doi.org/10.5194/esurf-4-359-2016

Fedele, J. J., & Paola, C. (2007). Similarity solutions for fluvial sediment fining by selective deposition. *Journal of Geophysical Research*, *112*(F2), F02038. https://doi.org/10.1029/2005JF000409

FOEN. (2024, 2025) Hydrological data. Federal Office for the Environment, Ittigen, Switzerland. Available from: https://www.hydrodaten.admin.ch/en/

Fonstad, M. A., Dietrich, J. T., Courville, B. C., Jensen, J. L., & Carbonneau, P. E. (2013). Topographic structure from motion: A new development in photogrammetric measurement. *Earth Surface Processes and Landforms*, *38*(4), 421–430. https://doi.org/10.1002/esp.3366

Garefalakis, P., do Prado, A. H., Mair, D., Douillet, G. A., Nyffenegger, F., & Schlunegger, F. (2023). Comparison of three grain size measuring methods applied to coarse-grained gravel deposits. *Sedimentary Geology*, *446*, 106340. https://doi.org/10.1016/j.sedgeo.2023.106340

GEKOBE. (2014) Gewässerentwicklungskonzept Bern. Strategische Planungen nach GSchG/GSchV: Sanierung des Geschiebehaushaltes im Kanton. Schlussbericht: Gewässersystem Sense–Saane–Aare. [Berne river development concept. Strategic planning according to WPA/WPO: mitigation of the bedload budget in the canton. Final report: Sense-Saane-Aare river system]. Bau-, Verkehrs- und Energiedirektion (BVE), Canton Bern; 19.

Glur, L., Wirth, S. B., Büntgen, U., Gilli, A., Haug, G. H., Schär, C., Beer, J., & Anselmetti, F. S. (2013). Frequent floods in the European Alps coincide with cooler periods of the past 2500 years. *Scientific Reports*, *3*(1), 2770. https://doi.org/10.1038/srep02770

GRANT, G. E., SWANSON, F. J., & WOLMAN, M. G. (1990). Pattern and origin of stepped-bed morphology in high-gradient streams, Western Cascades, Oregon. *GSA Bulletin*, *102*(3), 340–352. https://doi.org/10.1130/0016-7606(1990)102%253C0340:PAOOSB%253E2.3.CO;2

Gumbel, E. J. (1942). On the Frequency Distribution of Extreme Values in Meteorological Data. *Bulletin of the American Meteorological Society*, *23*(3), 95–105.

Gurnell, A. M., Bertoldi, W., & Corenblit, D. (2012). Changing river channels: The roles of hydrological processes, plants and pioneer fluvial landforms in humid temperate, mixed load, gravel bed rivers. *Earth-Science Reviews*, *111*(1), 129–141. https://doi.org/10.1016/j.earscirev.2011.11.005

Gurnell, A. M., Rinaldi, M., Belletti, B., Bizzi, S., Blamauer, B., Braca, G., Buijse, A. D., Bussettini, M., Camenen, B., Comiti, F., Demarchi, L., García de Jalón, D., González del Tánago, M., Grabowski, R. C., Gunn, I. D. M., Habersack, H., Hendriks, D., Henshaw, A. J., Klösch, M., … Ziliani, L. (2016). A multi-scale hierarchical framework for developing understanding of river behaviour to support river management. *Aquatic Sciences*, *78*(1), 1–16. https://doi.org/10.1007/s00027-015-0424-5

Habersack, H. M., Nachtneb El, H. P., & Laronne, J. B. (2001). The continuous measurement of bedload discharge in a large alpine gravel bed river. *Journal of Hydraulic Research*, *39*(2), 125–133. https://doi.org/10.1080/00221680109499813

Hohensinner, S., Egger, G., Muhar, S., Vaudor, L., & Piégay, H. (2021). What remains today of pre-industrial Alpine rivers? Census of historical and current channel patterns in the Alps. *River Research and Applications*, *37*(2), 128–149. https://doi.org/10.1002/rra.3751

James, M. R., Antoniazza, G., Robson, S., & Lane, S. N. (2020). Mitigating systematic error in topographic models for geomorphic change detection: Accuracy, precision and considerations beyond off-nadir imagery. *Earth Surface Processes and Landforms*, *45*(10), 2251–2271. https://doi.org/10.1002/esp.4878

James, M. R., & Robson, S. (2012). Straightforward reconstruction of 3D surfaces and topography with a camera: Accuracy and geoscience application. *Journal of Geophysical Research: Earth Surface*, *117*(F3), 2011JF002289. https://doi.org/10.1029/2011JF002289

Javernick, L., Brasington, J., & Caruso, B. (2014). Modeling the topography of shallow braided rivers using Structure-from-Motion photogrammetry. *Geomorphology*, *213*, 166–182. https://doi.org/10.1016/j.geomorph.2014.01.006

Kundzewicz, Z. W., Pińskwar, I., & Brakenridge, G. R. (2017). Changes in river flood hazard in Europe: A review. *Hydrology Research*, *49*(2), 294–302. https://doi.org/10.2166/nh.2017.016

Lane, S. N., Bakker, M., Gabbud, C., Micheletti, N., & Saugy, J.-N. (2017). Sediment export, transient landscape response and catchment-scale connectivity following rapid climate warming and Alpine glacier recession. *Geomorphology*, *277*, 210–227. https://doi.org/10.1016/j.geomorph.2016.02.015

Lane, S. N., Tayefi, V., Reid, S. C., Yu, D., & Hardy, R. J. (2007). Interactions between sediment delivery, channel change, climate change and flood risk in a temperate upland environment. *Earth Surface Processes and Landforms*, *32*(3), 429–446. https://doi.org/10.1002/esp.1404

https://doi.org/10.5194/egusphere-2025-5145
Preprint. Discussion started: 28 October 2025

Liu, Y., Zheng, H., & Zhao, J. (2025). Enhanced water quality prediction by LSTM and graph attention network (L-GAT): An analytical study of the Pearl River Basin. *Water Research X*, *28*, 100383. https://doi.org/10.1016/j.wroa.2025.100383

Lobanova, A., Liersch, S., Nunes, J. P., Didovets, I., Stagl, J., Huang, S., Koch, H., Rivas López, M. del R., Maule, C. F., Hattermann, F., & Krysanova, V. (2018). Hydrological impacts of moderate and high-end climate change across European river basins. *Journal of Hydrology: Regional Studies*, *18*, 15–30. https://doi.org/10.1016/j.ejrh.2018.05.003

MacKenzie, L. G., Eaton, B. C., & Church, M. (2018). Breaking from the average: Why large grains matter in gravel-bed streams. *Earth Surface Processes and Landforms*, *43*(15), 3190–3196. https://doi.org/10.1002/esp.4465

Madej, M. A. (1999). Temporal and spatial variability in thalweg profiles of a gravel-bed river. *Earth Surface Processes and Landforms*, *24*(12), 1153–1169. https://doi.org/10.1002/(SICI)1096-9837(199911)24:12%253C1153::AID-ESP41%253E3.0.CO;2-8

Mair, D., Do Prado, A. H., Garefalakis, P., Lechmann, A., Whittaker, A., & Schlunegger, F. (2022a). Grain size of fluvial gravel bars from close-range UAV imagery – uncertainty in segmentation-based data. *Earth Surface Dynamics*, *10*(5), 953–973. https://doi.org/10.5194/esurf-10-953-2022

Mair, D., Do Prado, A. H., Garefalakis, P., Lechmann, A., Whittaker, A., & Schlunegger, F. (2022b). Grain size of fluvial gravel bars from close-range UAV imagery – uncertainty in segmentation-based data. *Earth Surface Dynamics*, *10*(5), 953–973. https://doi.org/10.5194/esurf-10-953-2022

Mair, D., Do Prado, A. H., Garefalakis, P., Lechmann, A., Whittaker, A., & Schlunegger, F. (2022c). Grain size of fluvial gravel bars from close-range UAV imagery – uncertainty in segmentation-based data. *Earth Surface Dynamics*, *10*(5), 953–973. https://doi.org/10.5194/esurf-10-953-2022

Mair, D., Witz, G., Do Prado, A. H., Garefalakis, P., & Schlunegger, F. (2024). Automated detecting, segmenting and measuring of grains in images of fluvial sediments: The potential for large and precise data from specialist deep learning models and transfer learning. *Earth Surface Processes and Landforms*, *49*(3), 1099–1116. https://doi.org/10.1002/esp.5755

Miazza, R., Pascal, I., & Ancey, C. (2024). Automated grain sizing from uncrewed aerial vehicles imagery of a gravel-bed river: Benchmarking of three object-based methods. *Earth Surface Processes and Landforms*, *49*(5), 1503–1514. https://doi.org/10.1002/esp.5782

Minár, J., Drăguţ, L., Evans, I. S., Feciskanin, R., Gallay, M., Jenčo, M., & Popov, A. (2024). Physical geomorphometry for elementary land surface segmentation and digital geomorphological mapping. *Earth-Science Reviews*, *248*, 104631. https://doi.org/10.1016/j.earscirev.2023.104631

Molnar, P., & Burlando, P. (2008). Variability in the scale properties of high-resolution precipitation data in the Alpine climate of Switzerland. *Water Resources Research*, *44*(10), 2007WR006142. https://doi.org/10.1029/2007WR006142

Montgomery, D. R., & Buffington, J. M. (1997). Channel-reach morphology in mountain drainage basins. *Geological Society of America Bulletin*, *109*(5), 596–611. https://doi.org/10.1130/0016-7606(1997)109%253C0596:CRMIMD%253E2.3.CO;2

Moreira, L. L., De Brito, M. M., & Kobiyama, M. (2021). Effects of Different Normalisation, Aggregation, and Classification Methods on the Construction of Flood Vulnerability Indexes. *Water*, *13*(1), 98. https://doi.org/10.3390/w13010098

Newson, Malcolm. D., & Large, A. R. G. (2006). 'Natural' rivers, 'hydromorphological quality' and river restoration: A challenging new agenda for applied fluvial geomorphology. *Earth Surface Processes and Landforms*, *31*(13), 1606–1624. https://doi.org/10.1002/esp.1430

Nicholas, A. (2013). Morphodynamic diversity of the world's largest rivers. *Geology*, *41*(4), 475–478. https://doi.org/10.1130/G34016.1

O'Briain, R. (2019). Climate change and European rivers: An eco-hydromorphological perspective. *Ecohydrology*, *12*(5), e2099. https://doi.org/10.1002/eco.2099

Pachitariu, M., Rariden, M., & Stringer, C. (2025). *Cellpose-SAM: Superhuman generalization for cellular segmentation* (p. 2025.04.28.651001). bioRxiv. https://doi.org/10.1101/2025.04.28.651001

Paola, C., & Seal, R. (1995). Grain Size Patchiness as a Cause of Selective Deposition and Downstream Fining. *Water Resources Research*, *31*(5), 1395–1407. https://doi.org/10.1029/94WR02975

Parker, G. (1990). Surface-based bedload transport relation for gravel rivers. *Journal of Hydraulic Research*, *28*(4), 417–436. https://doi.org/10.1080/00221689009499058

Patel, N. K., Schlunegger, F., Mair, D., Pati, P., do Prado, A. H., Garefalakis, P., & Choudhury, R. K. (2025). Source-to-sink patterns of grain size along the Yamuna River in the Indian Himalaya. *Geomorphology*, *486*, 109909. https://doi.org/10.1016/j.geomorph.2025.109909

Phillips, C. B., & Jerolmack, D. J. (2016). Self-organization of river channels as a critical filter on climate signals. *Science*, *352*(6286), 694–697. https://doi.org/10.1126/science.aad3348

https://doi.org/10.5194/egusphere-2025-5145
Preprint. Discussion started: 28 October 2025

Ribet, L., Liébault, F., Borgniet, L., Deschâtres, M., & Melun, G. (2025). Surface grain-size mapping of braided channels from SfM photogrammetry. *Earth Surface Dynamics*, *13*(4), 607–627. https://doi.org/10.5194/esurf-13-607-2025

Rice, S. P., & Church, M. (2010). Grain-size sorting within river bars in relation to downstream fining along a wandering channel. *Sedimentology*, *57*(1), 232–251. https://doi.org/10.1111/j.1365-3091.2009.01108.x

Saisana, M., & Saltelli, A. (2011). Rankings and Ratings: Instructions for Use. *Hague Journal on the Rule of Law*, *3*(02), 247–268. https://doi.org/10.1017/s1876404511200058

Schlunegger, F., Delunel, R., & Garefalakis, P. (2020). Short communication: Field data reveal that the transport probability of clasts in Peruvian and Swiss streams mainly depends on the sorting of the grains. *Earth Surface Dynamics*, *8*(3), 717–728. https://doi.org/10.5194/esurf-8-717-2020

Schwanghart, W., & Scherler, D. (2017). Bumps in river profiles: Uncertainty assessment and smoothing using quantile regression techniques. *Earth Surface Dynamics*, *5*(4), 821–839. https://doi.org/10.5194/esurf-5-821-2017

Slater, L. J., Villarini, G., & Bradley, A. A. (2017). Weighting of NMME temperature and precipitation forecasts across Europe. *Journal of Hydrology*, *552*, 646–659. https://doi.org/10.1016/j.jhydrol.2017.07.029

Steiger, J., Tabacchi, E., Dufour, S., Corenblit, D., & Peiry, J. -L. (2005). Hydrogeomorphic processes affecting riparian habitat within alluvial channel–floodplain river systems: A review for the temperate zone. *River Research and Applications*, *21*(7), 719–737. https://doi.org/10.1002/rra.879

Stringer, C., Wang, T., Michaelos, M., & Pachitariu, M. (2021). Cellpose: A generalist algorithm for cellular segmentation. *Nature Methods*, *18*(1), 100–106. https://doi.org/10.1038/s41592-020-01018-x

Surian, N., Righini, M., Lucía, A., Nardi, L., Amponsah, W., Benvenuti, M., Borga, M., Cavalli, M., Comiti, F., Marchi, L., Rinaldi, M., & Viero, A. (2016). Channel response to extreme floods: Insights on controlling factors from six mountain rivers in northern Apennines, Italy. *Geomorphology*, *272*, 78–91. https://doi.org/10.1016/j.geomorph.2016.02.002

swipos: Swiss Positioning Service. (2024) Available from: https://www.swisstopo.admin.ch/en/geodata/geoservices/swipos.html

swisstopo. (2024) Mapping platform of the Federal Office of Topography, swisstopo. Available from: https://map.geo.admin.ch

Tonolla, D., Geilhausen, M., & Doering, M. (2021). Seven decades of hydrogeomorphological changes in a near-natural (Sense River) and a hydropower-

https://doi.org/10.5194/egusphere-2025-5145
Preprint. Discussion started: 28 October 2025

regulated (Sarine River) pre-Alpine river floodplain in Western Switzerland. *Earth Surface Processes and Landforms*, *46*(1), 252–266. https://doi.org/10.1002/esp.5017

Vázquez-Tarrío, D., Borgniet, L., Liébault, F., & Recking, A. (2017). Using UAS optical imagery and SfM photogrammetry to characterize the surface grain size of gravel bars in a braided river (Vénéon River, French Alps). *Geomorphology*, *285*, 94–105. https://doi.org/10.1016/j.geomorph.2017.01.039

Venditti, J. G., Nelson, P. A., Minear, J. T., Wooster, J., & Dietrich, W. E. (2012). Alternate bar response to sediment supply termination. *Journal of Geophysical Research: Earth Surface*, *117*(F2). https://doi.org/10.1029/2011JF002254

Vericat, D., Wheaton, J. M., & Brasington, J. (2017). Revisiting the Morphological Approach. In *Gravel-Bed Rivers* (pp. 121–158). John Wiley & Sons, Ltd. https://doi.org/10.1002/9781118971437.ch5

Viviroli, D., & Weingartner, R. (2004). The hydrological significance of mountains: From regional to global scale. *Hydrology and Earth System Sciences*, *8*(6), 1017–1030. https://doi.org/10.5194/hess-8-1017-2004

Warburton, J., & Davies, T. (1994). Variability of bedload transport and channel morphology in a braided river hydraulic model. *Earth Surface Processes and Landforms*, *19*(5), 403–421. https://doi.org/10.1002/esp.3290190503

Weingartner, R., & Aschwanden, H. (1994). *Quantification des débits des cours d'eau des Alpes suisses et des influences anthropiques qui les affectent*. https://doi.org/10.3406/rga.1994.3749

Westoby, M. J., Brasington, J., Glasser, N. F., Hambrey, M. J., & Reynolds, J. M. (2012). 'Structure-from-Motion' photogrammetry: A low-cost, effective tool for geoscience applications. *Geomorphology*, *179*, 300–314. https://doi.org/10.1016/j.geomorph.2012.08.021

Wheaton, J. M., Brasington, J., Darby, S. E., & Sear, D. A. (2010). Accounting for uncertainty in DEMs from repeat topographic surveys: Improved sediment budgets. *Earth Surface Processes and Landforms*, *35*(2), 136–156. https://doi.org/10.1002/esp.1886

Wilcock, P. R., & Crowe, J. C. (2003). Surface-based Transport Model for Mixed-Size Sediment. *Journal of Hydraulic Engineering*, *129*(2), 120–128. https://doi.org/10.1061/(ASCE)0733-9429(2003)129:2(120)

Wilcock, P. R., & McArdell, B. W. (1993). Surface-based fractional transport rates: Mobilization thresholds and partial transport of a sand-gravel sediment. *Water Resources Research*, *29*(4), 1297–1312. https://doi.org/10.1029/92WR02748

Wolman, M. G. (1954). A method of sampling coarse river-bed material. *Transactions, American Geophysical Union*, *35*(6), 951. https://doi.org/10.1029/TR035i006p00951

https://doi.org/10.5194/egusphere-2025-5145
Preprint. Discussion started: 28 October 2025

Wolman, M., & Leopold, L. (1957). *River flood plains: Some observations on their formation* (Report No. 282C; Professional Paper, pp. 87–109). USGS Publications Warehouse. https://doi.org/10.3133/pp282C

Woodget, A. S., & Austrums, R. (2017). Subaerial gravel size measurement using topographic data derived from a UAV-SfM approach. *Earth Surface Processes and Landforms*, *42*(9), 1434–1443. https://doi.org/10.1002/esp.4139

Woodget, A. S., Carbonneau, P. E., Visser, F., & Maddock, I. P. (2015). Quantifying submerged fluvial topography using hyperspatial resolution UAS imagery and structure from motion photogrammetry. *Earth Surface Processes and Landforms*, *40*(1), 47–64. https://doi.org/10.1002/esp.3613